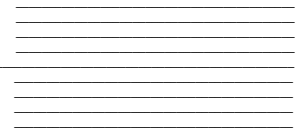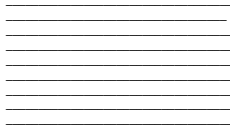# Improving the Payload Capacity of Continuum Robots through Robot Joining

by

Ryan Zazo

Supervisor: Jessica Burgner-Kahrs
April 2023

B.A.Sc. Thesis

Division of Engineering Science
UNIVERSITY OF TORONTO

Engineering Science Thesis

Improving the Payload Capacity of Continuum
Robots through Robot Joining

Author: Ryan Zazo

Supervisor: Jessica Burgner-Kahrs

UNIVERSITY OF
TORONTO

continuum
robotics lab

April 21$^{\text{st}}$ 2023

Student Number: 1004906890

Abstract

This work aims to enable continuum robots to be used as a viable solution in untapped fields, such as aircraft maintenance. The use of continuum robots in aircraft maintenance will be complicit in reducing the overall downtime and costs associated with jet-engine maintenance thereby enabling more frequent inspection and maintenance of said engines. This work proposes a novel continuum robot joining mechanism, enabling multiple continuum individual continuum robots to traverse in an aircraft engine and then combine into a stiffer system. The proposed mechanism has a maximum failure load of 29.43 N, weighing in at less than 4.60g and having a height, length and width of 15.53 mm x 30 mm x 12.5 mm.

Acknowledgements

I wish to thank Professor Burgner-Kahrs for the opportunity to pursue my undergraduate thesis at the Continuum Robotics Lab. This experience has enabled me to learn more about continuum robots and working in robotics academia.

I wish to also thank Chloe Pogue for the immense help she has provided me over the course of this project, having helped guide me on the right path while also giving me the freedom to explore my own solutions.

I would also like to thank all my friends and family that have been very supportive throughout this process.

Contents

List of Figures

List of Tables

1 Introduction

Tendon driven continuum robots provide increased maneuverability compared to traditional rigid link serial robots, enabling them to navigate through small and confined spaces [1]. Tendon driven continuum robots are composed of disks connected by a flexible rod which acts as the robot's backbone and are controlled by tendons located concentrically around the backbone and terminating at the end of each robot segment. By releasing or pulling on the tendons, the robot's various segments assume different curvatures enabling the robot to assume complex shapes. Current continuum robot designs function well in cluttered environments over small distances as they offer many degrees of freedom, are dexterous and are compliant to their environment as demonstrated in continuum robotics research aimed at medical applications [2], [3]. However, for large-scale operations that require robots with very small diameters and long lengths, such as jet-engine inspection and maintenance, continuum robots have inadequate payload capacities, accuracy and precision. Various research institutes have experimented with designing continuum robots to complete the task of aircraft engine maintenance, but have faced the aforementioned limitations [4].

A proposal such as using multiple continuum robots and connecting them using a shape-memory-allow (SMA) based joining mechanisms has been proposed, but does not fully address the problem. For instance, it takes 36 seconds to actuate the mechanism [4] which makes for long wait times when undertaking simple readjustments. Also, the SMA mechanism can only withstand loads of up to 10 N [4], limiting the payload capacity of the combined system which in turn limits what operations the system can perform in a maintenance task. Finally, this system results in a maximum deflection of 5.1% [4], which is rather large when considering the size of jet-engines and the tolerances required when maintaining them.

The payload capacity of continuum robots can be improved from current mechanisms, by allowing multiple continuum robots to join together and provide structural support to a main "task-completing" robot. This would be accomplished by designing a novel joining mechanism and will enable the system to perform precise tasks such as machining and maintenance of aircraft engines over long distances.

This work aims to design a novel mechanical lock mechanism to enable support con-

tinuum robots to join to a task-completing robot's body, resulting in greater payload capacities than the individual robots. In addition, this work aims to design a joining mechanism to enable a task-completing robot perform tasks such as machine aircraft grade aluminum with a number 6 drill bit, metal grinding, engine coating repair and safety inspection. Machining aircraft grade aluminum requires withstanding axial thrust forces estimated at 235.4 N , whereas grinding materials requires withstanding radial forces of up to 1.5 N [5], [6]. Finally this work aims to lower the maximum deflection experienced by a continuum robot to less than 1% maximum deflection [7], to enable precise and accurate machining.

The designed mechanisms will be evaluated for their maximum-load bearing capacity when engaged in various orientations, to simulate operation in confined environments where alignment is not guaranteed to be ideal.

This work aims to enable continuum robots to be used as a viable solution in untapped fields, such as aircraft maintenance. The use of continuum robots in aircraft maintenance will be complicit in reducing the overall downtime and costs associated with jet-engine maintenance thereby enabling more frequent inspection and maintenance of said engines.

2 Literature Review

The use of collaborative continuum robots to improve payload capacity for aircraft maintenance is novel, however research has been done to use continuum robots independently for aircraft maintenance [4], [7], [8], [9], [10], [11]. In addition to this, the concept of collaborative continuum robots has been explored through the use of Parallel Continuum Robots (PCR) [12], [13]. Work has also been done to improve the payload capacity of individual continuum robots through the use continuum robot variable stiffness mechanisms [15].

2.1 Aircraft Engine Maintenance and Repair Using Continuum Robots

Researchers have been experimenting with continuum robots for aircraft maintenance and inspection. Example tasks include aircraft engine turbine blade repair, engine coating repair and tasks pertaining to safety inspection for these engines [4], [7], [8], [9], [10],

[11]. To perform these tasks within an aircraft engine, the robot must have a diameter of less than 15 mm to fit within the access ports to reach the insides of the aircraft engine without disassembly [4],[10]. Given the overall size of aircraft engines, continuum robots aiming to perform maintenance and inspection for an engine such as the Rolls-Royce Trent XWB are required to be at least 1200 mm long [8].

Researchers from the Rolls-Royce University Technology Center at the University of Nottingham have worked extensively on this topic and have produced many papers, as such this portion of the literature review will be discussing the results from 6 representative works.

2.1.1 Individual Continuum Robots for Aircraft Maintenance

Dong et al.'s paper serves to set up the requirements for a continuum robot system to be used for inspection and repair tasks of aircraft engines and proposes a conforming design [8]. The paper outlines requirements for a continuum robot servicing a particular jet engine, the Rolls-Royce Trent XWB: an overall arm length of 1200 mm of which for the last 400 mm, the robot must have a maximum diameter of 15 mm. The robot must also be able to carry a payload of 0.250 g to carry a spindle and be able to bend at least $\pm 90°$ per section [8]. A section refers to a region of the continuum robot all controlled by the same tendons. The requirements stipulate that the sections must be between 150 mm and 50 mm long.

The proposed solution managed to achieve ± 10 mm error when following a 1000 mm long path with multiple bends between $\pm 45°$ and $\pm 90°$. At full length while carrying a 200 g load at its tip, the robot deflected 21.1 mm.

Following this first paper, in 2018, Dong et al. published a follow up paper which aimed to demonstrate the viability of continuum robots for repair and maintenance tasks in small confined spaces, such as aircraft engines [9]. In it, Dong et al. demonstrated that by using a single 300 mm long continuum robot, it is possible to perform machining tasks accurate to within ± 0.5 mm [9]. It is important to note that the machining they performed resulted in removing "a scallop shape material" from the work-piece, by passing over the section and removing a small amount per pass, see figure 1, [9]. According to Alatorre et al., grinding only requires withstanding radial forces of up to 1.5 N, whereas drilling through aircraft grade aluminum directly, using a number 6 drill bit, requires the

robot to withstand 235.4 N of axial forces [6], [5].
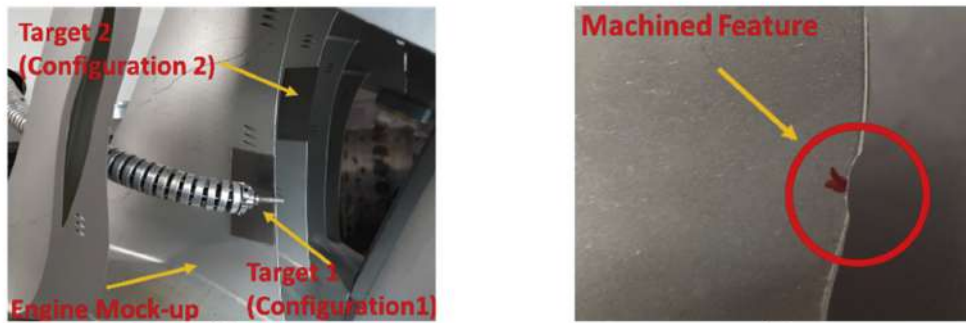
Figure 1: Continuum Robot machining an aluminum work-piece [9]

2.1.2 Collaborative Continuum Robots For Aircraft Maintenance

Following the previous papers, the researchers at the University of Nottingham have proposed a paradigm shift to using multiple collaborative continuum robots for aircraft inspection and maintenance.

One paper from the group proposed the use of an auxiliary continuum robot with a camera, referred to as the observer, to provide feedback for the task completing robot, the adder [11]. The observer also has laser diodes to ensure it is at the correct distance from the walls, which helps with the overall accuracy of the system [11]. See figure 2 for an illustration of this system. This combined system however does not provide much in the way of increasing the maximum payload capacity and decreasing the system's deflection, but does provide some extra feedback for the motor control. The application in this paper was coating repairs, which does not require high precision control, rather the system needs to be near the target and then spray it [11]. By having 2 robots working together, the observer was given all the sensitive equipment while the adder was given only the tools to carry out the tasks, as they take up space that would otherwise be allocated for cameras and other temperature-sensitive equipment.
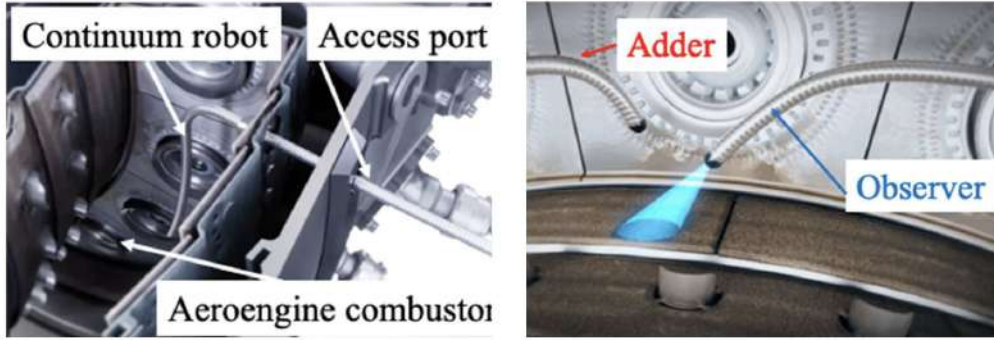
Figure 2: Adder and Observer CRs working together [11]

Following this paper, Russo et al. proposed joining robots together to accomplish aircraft maintenance tasks. They then proposed a novel joining mechanism using shape-memory-alloy (SMA). SMA is a special alloy that "saves" a shape and can revert back to it when cooled down. In this mechanism, when heating up the SMA, the grasping element opens, allowing a coupling element to be held by the grasping element when it cools back down. See Figure 3 for a description of how the mechanism works. The paper then presents their results, having implemented this SMA based locking mechanism on two continuum robots, one bearing the grasping element and the other the coupling one. Results from this experiment have shown a 200% stiffness increase and a reduction of 70% of the deflection under load in the combined robot systems in comparison to the individual robots [4].
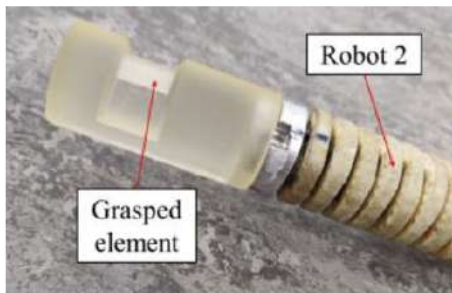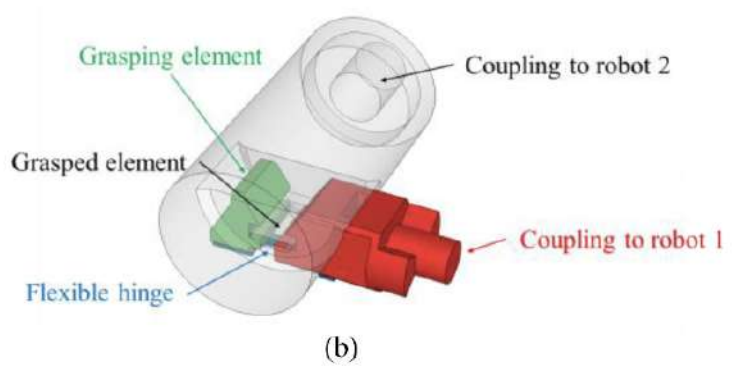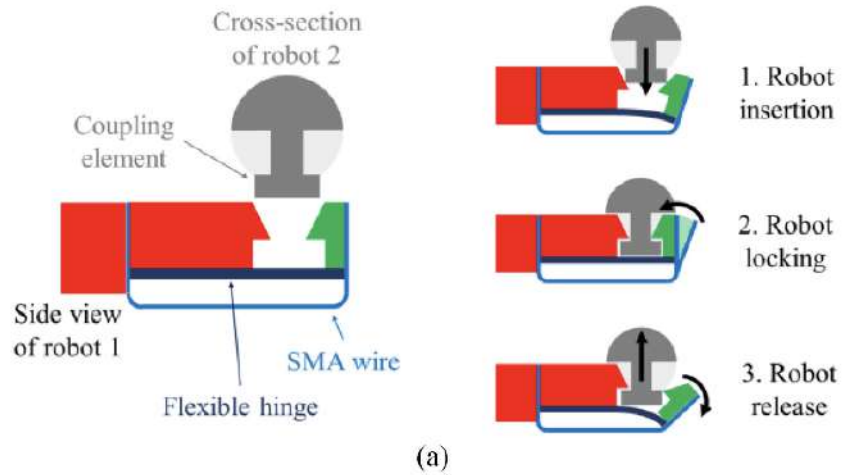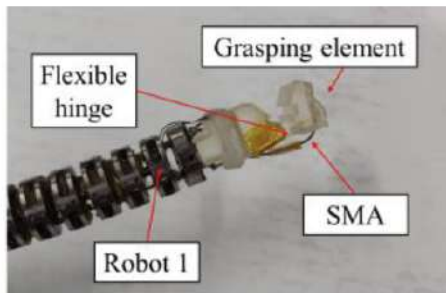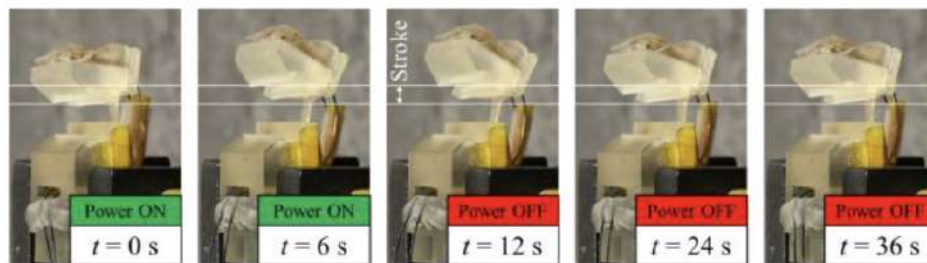
Figure 3: Drawing and simulation of the SMA based locking mechanism [4]

As presented in the introduction, this mechanism faces limitation such as taking 36

seconds to complete a grasping actuation, having a theoretical maximum load of 10 N and a maximum deflection of 5.1% at full extension [4].

2.1.3 Limitations of Continuum Robots used for Aircraft Maintenance

Currently, the status quo in continuum robots aimed at aircraft maintenance tasks can complete regular inspection tasks, just like endoscopes, but are not ready for complex machining tasks. The current problems are two-fold; both in payload capacity and accuracy.

First, as stated previously, both the individual and combined continuum robot systems have a low payload capacity, too low to perform a general machining task. To perform machining tasks on aircraft grade aluminum, the system must be able to withstand 235.4 N of axial forces [5]. As of now, the individual continuum robot has a payload capacity of 0.250g at the tip (equivalent to roughly 2.5 N), whereas the combined continuum robot system has a theoretical maximum payload capacity of 10 N [8], [4], [9].

Next, there is the problem of accuracy; minimizing the deflection at full length will ensure that any maintenance tasks undertaken can be done with precision and accuracy to minimize errors in the maintenance and require further corrections. Both of the current types of solutions are inaccurate; the individual continuum robot has an error of ±10 mm when extended 1000 mm, whereas the combined continuum robot system achieves a deflection of 5.1% at full extension (also 1000 mm).

2.2 Parallel Continuum Robots

Researchers in continuum robotics have worked extensively to design *Parallel Continuum Robots* (PCR), which are continuum robots made up of multiple continuum chains coupled to a common end-effector. This design is meant to leverage the redundancy provided by having multiple links be actuated at once to perform a movement, to increase the positional accuracy and increase reliability, all while providing higher payload capacities [12], [13]. These qualities make them ideal in settings requiring accuracy and repeatability such as manufacturing environments.
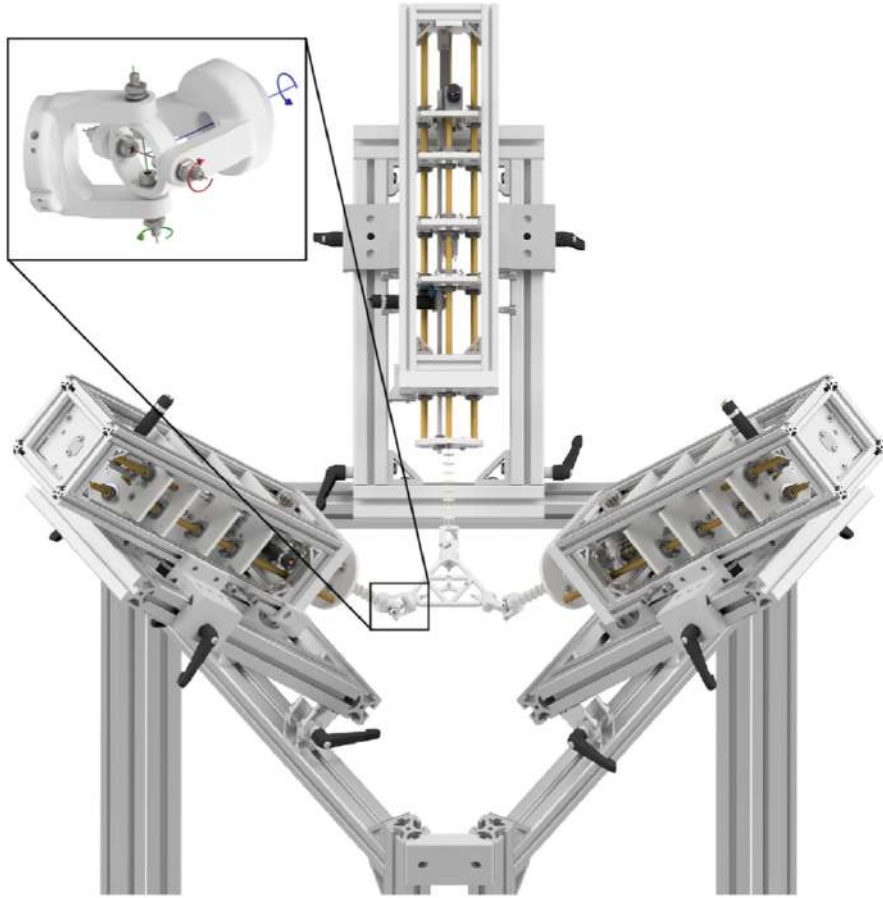
Figure 4: 3D model of a PCR robot [13].

2.2.1 Planar Parallel Continuum Robots

Nuelle et al.'s paper introduces a novel planar PCR, demonstrating a repeatability of 1.0% and a positional accuracy of 1.4% relative to one continuum segment length [12]. Although these are impressive feats, this planar PCR only enables movement in a single 2D plane, which is not ideal in maintenance tasks where full range of motion is required. See figure 5 for a picture of the designed planar PCR.

In addition to this, the continuum chains of such a Planar PCR design are rigidly attached to the end effector at angles of $\frac{2\pi}{3}$ apart, with the base of the chains equally distributed on a circle with radius r_{base} [12]. The resulting workspace occupies a subsection of the area of the circle of radius r_{base} connecting the continuum chains' bases. This is not ideal in environments as large as aircraft engines, with engines with sizes on the order of meters, as this would require the construction of multiple continuum chains of

comparable length, resulting in a large deflection.

Figure 5: Planar PCR design [12]

2.2.2 Reconfigurable Parallel Continuum Robots

Boëtcher et al's paper describes the design of another kind of Parallel Continuum Robot called a Reconfigurable PCR. Similar to the Planar PCR, it's made up of 3 continuum chains attached to a common end-effector platform [13]. This reconfigurable PCRs can also change the position of the base-pose of the continuum chains [13]. See figure 4 for a 3D rendering of this design.

When coupled as a PCR, continuum chains individually capable of positioning and heading repeatability of 5.5 mm in position and 3.2° in orientation can achieve positioning and heading repeatabilities of 3.3 mm and 1.2° together.

Unlike Planar PCRs, in this design each continuum kinematic chain has 3 degrees of freedom, resulting in a PCR with 9 total degrees of freedom, 3 of which being redundant [13]. These extra degrees of freedom enable the robot to have a much broader task space then their planar counterparts. Just like with the Planar PCRs, the continuum chains of such a PCR design are rigidly attached to the end effector at angles of $\frac{2\pi}{3}$ apart, meaning that the resulting workspace has to fall between the base of each of the continuum chains. Once again, this is not ideal as this means that in environments requiring large workspaces on the order of meters, such as aircraft engines, the kinematic chains also have to be of comparable length, which results in large deflections.

2.2.3 Limitations of Parallel Continuum Robots

To attach the continuum chains to the end-effector, PCR designs use revolute joints [12], [13]. This does not allow unlocking/unhinging of the joints, requiring that the system

be fully "engaged" prior to the use of the robot. This makes the PCR design effectively impossible to use in environments such as jet engines where the chains must enter the environment from different sides and meet in the middle.

Even if we can instead have all continuum chains and the end effector fit within the same access port at the same time, given the diameter of the access ports, each individual chain must have a proportionally smaller diameter. Given the relationship between the stiffness of a continuum chain and the deflection observed, this will result in a system that deflects more, hence undermining the advantages of using a PCR in the first place [8]. As such, for this application, a functioning design should aim to incorporate mechanisms that enable the continuum links to join inside of the environment to circumvent the limitations imposed by small access port diameters.

2.3   Variable Stiffness Mechanisms in Continuum Robots

Beyond techniques utilizing multiple continuum robots, researchers have also been looking into techniques to make their continuum robots stiffer when desired. In fields such as aircraft maintenance, this is important as it enables the continuum robot to be flexible when traversing the environment and stiffen up when accomplishing force-intensive tasks such as machining aluminum. Although there are many different approaches to variable stiffness mechanisms in continuum robots, 2 representative techniques will be explored in this literature review, mainly SMA-based mechanisms and jamming.

2.3.1   SMA Based Variable Stiffness

Researchers have developed techniques to stiffen a robot through the use of mechanical mechanisms. Yang et al. presents a variable stiffness mechanism, which works by introducing locking mechanisms actuated by SMA springs between disks of the continuum robot [15]. By actuating the SMA spring and then locking the mechanism, the section length is preserved, increasing the stiffness of the robot. This mechanism enabled Yang et al. to achieve positioning errors of less than 2.33% of the robot's length at the end-effector [15]. See figure 6 for an illustration of the system.
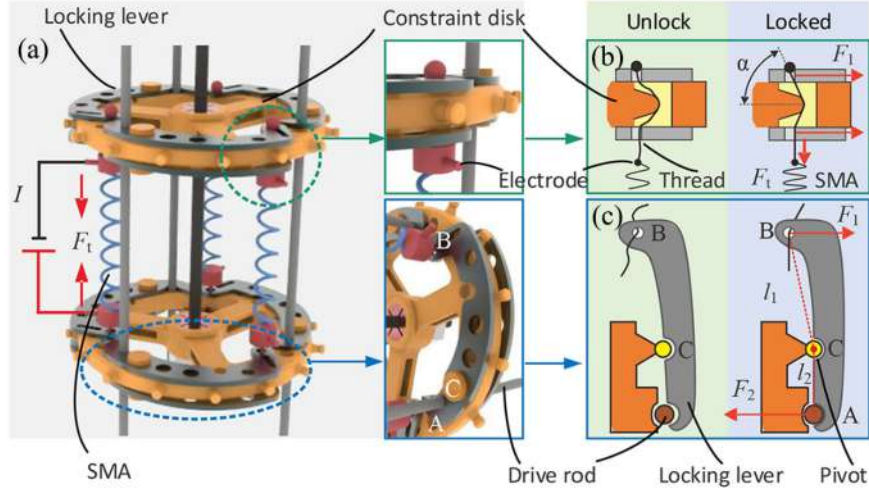
Figure 6: SMA-based locking mechanism [15]

2.3.2 Jamming

Jamming is a technique that controls the stiffness of a continuum robot by controlling the friction between parts of the robot, usually by means of controlling air pressure. Jamming can be further subdivided into two separate methods; particle jamming and layer jamming.

Particle jamming is a technique that has small particles within a elastic membrane, that when the pressure is decreased, they press together leading to increased stiffness of the continuum robot [16], [17]. Li et al. proposed a novel particle jamming design which uses 3 flexible air-filled chambers that are pre-charged with air, surrounding the spine containing the particles[17]. The use of the pre-charged air chambers enabled the design to not use heavy air compressors and valves [17]. To increase the stiffness of the robot, this method compresses the robot to increase the pressure of the air chambers. The paper then measured the deflection resulting from different lateral and axial forces on their design when using different pressures for the air filled chamber; Li et al. found that an increase in pre-charged air pressure resulted in lateral and axial stiffness increases [17]. See figure 7 for a picture of the proposed mechanism.

Layer jamming on the other hand uses layers of overlapping material to jam instead of particles. Here the robot has an outer and inner elastic membrane, with air between them. When the air between the layers gets sucked out, the outer layer collapses on the inner one and increases the stiffness of the robot. Langer et al. have found that layer
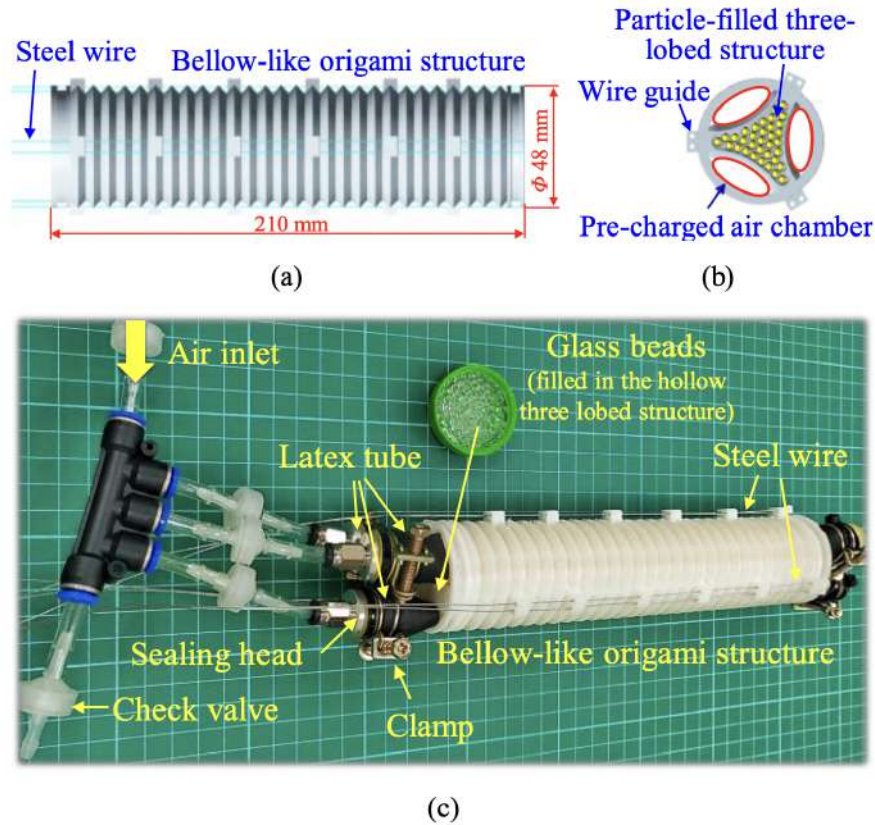
Figure 7: Continuum robot utilizing a particle jamming based variable stiffness mechanism [17]

jamming can permit even higher stiffness than particle jamming, when under vacuum, resulting in higher forces being required to achieve a deflection of 8.75mm axially and 10 mm laterally [16]. See figure 8 for a comparison of layer jamming and particle jamming (referred to as granular jamming here).

2.3.3 Limitations of Variable Stiffness Mechanisms

Although these mechanisms enable robots to increase and decrease their stiffness, they are not without their own problems. The biggest of which is the overall size of such mechanisms. The SMA based variable stiffness mechanism proposed by Yang et al. was implemented on a continuum robot with a diameter of 38mm, which is much larger than the 15mm diameter of access ports on aircraft engines [4], [15].

Jamming solutions require including auxiliary chambers filled with highly pressurized air, which increases the robots' diameter. Li et al's continuum robot has a diameter of 48mm and , which is too big to fit in any access ports present in aircraft engines [4],[17].
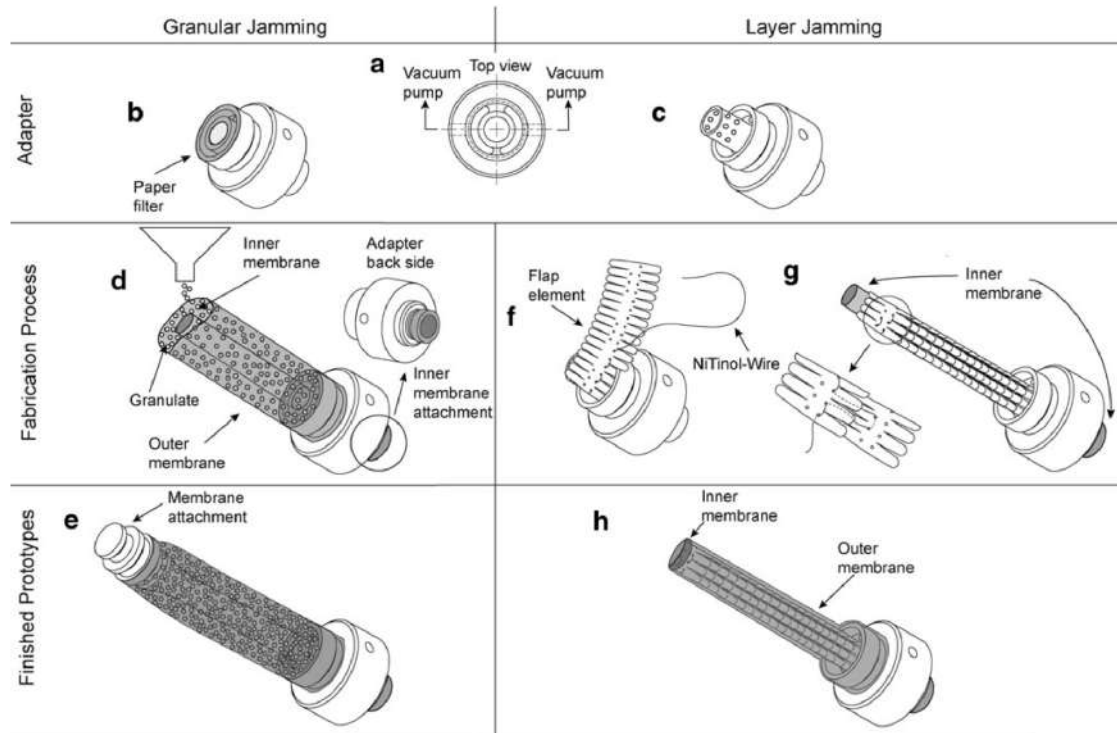
Figure 8: Comparison of Layer and Particle (called Granular) jamming [16]

To make these variable stiffness mechanisms viable in aircraft engine maintenance, they would need to be miniaturized, which may not be possible due to the size limitations of the components used.

In addition to this, these variable stiffening mechanisms add significant weight to the overall continuum robot's design, which can be problematic for longer continuum robots, such as the ones required for aircraft engine maintenance. This extra weight would add extra deflection in the robot that would need to be accounted for.

2.4   Literature Review Synthesis

This literature review explored various techniques and mechanisms that can be used to improve the payload capacity and stiffness of continuum robots, both in general and for aircraft maintenance tasks.

Current designs for continuum robots used for aircraft maintenance as of now provide little payload capacity at the robot's tip and low accuracy, but can be used within the environment [8], [4], [9]. To use collaborative continuum robots for aircraft maintenance, the joining mechanism explored will require a higher payload capacity.

The PCR design does not work in this environment either, as they do not fit within

aircraft access ports by design; the continuum chains must already be attached to the end-effector platform, but its not possible to insert the design inside of aircraft engines without taking apart the engine and building the robot within it. As such, for this application, a functioning design should aim to incorporate mechanisms that enable the continuum links to join inside of the environment to circumvent the limitations imposed by small access port diameters.

Variable stiffness mechanisms such as SMA base mechanisms and particle jamming are currently too large to be used effectively in continuum robots and will as such require significant work before being miniaturized enough to fit in an aircraft access port.

From this literature review, there is a potential avenue for further development for continuum robots for aircraft maintenance by utilizing robot joining. We can establish a set of objectives, metrics, criteria and constraints for a proposed solution.

2.4.1   Objectives, Metrics, Criteria and Constraints

The first objective of this design is ensuring that the mechanical lock design is fault-tolerant. This objective aims to improve the usability of the mechanism in complex and cluttered environments, by ensuring that it will self-adjust instead of requiring precise readjustments. The fault-tolerance of a design can be improved by increasing the symmetries present in the design and designing self-aligning mechanisms.

In addition to the above, having a payload capacity of 235.4 N or greater is desired to enable the collaborative continuum robot system perform tasks such as machining aluminum [5]. A higher payload capacity enables the design to be useful in a variety of force-intensive tasks, such as in aircraft maintenance or machining. To be comparable to the current state of the art, the mechanism must be able to withstand a maximum failure load of at least 10 N [4]. The payload capacity can also be increased through the support of more robots; therefore having a design that can support multiple helper robots collaborating with a single task-completing robot is ideal.

Although it is not explicitly stated as an objective, a faster actuation time is desirable, as it will enable rapid readjustments of the continuum robots' orientations. The designs can be evaluated based on the time it takes to actuate the mechanism and how long it takes to disengage the mechanism. To be comparable to the State of The Art solutions, the mechanism must actuate in less than 12 seconds, and disengage in less than 24 seconds

[4].

Finally, the design should improve the task-completing continuum robot's performance. The objective encompasses observing a tangible improvement to both the deflection and load capacity. Minimizing the weight and the size of the design both help in this respect. A lighter design will result in less deflection at the end-effector of the system. A smaller design will permit the individual robots navigate tight spaces. For the design to fit within the access ports of an aircraft engine, it must have a diameter of less than 15mm. As this is a preliminary design, this constraint has been relaxed to require the mechanism to be smaller than 20 mm in length, width and height. This was chosen to simplify the miniaturization task and to serve as a proof of concept. This will be discussed further in section 8.

The objectives, metrics, criteria and constraints are summarized in table 1.

All designs will be evaluated based on these objectives and criteria.

Objectives	Metrics	Criteria	Constraint
Faster Actuation Time	Time to Actuate the mechanism	Less is Better	Less than 12 seconds
	Time to Disengage the mechanism	Less is Better	Less than 24 seconds
Fault-Tolerant Mechanism	Symmetry of Design	More is better	
	Presence of Self-Aligning Mechanism	Yes is preferred	
High Payload Capacity	Failure Load Capacity	Load in Newtons	At least 10 N
	Number of helper robots that can attach to a task-completing robot	More is Better	At least 1
Improve the Task Completing Continuum Robot's Performance	Mechanism's Size (H, W, L) (in mm)	Smaller is better	Must be less than 20 mm in Length, Width and Height
	Total System Weight (in g)	Less is better	
	Difference in Task-completing robot Deflection with and without mechanism	Better performance with mechanism is better	Must be better than individual robot
	Difference in Maximum Load Capacity of Task-completing robot with and without mechanism	Better performance with mechanism is better	Must be better than individual robot

Table 1: Mechanism's design Objectives, Metrics, Criteria and Constraints

3 Design Work

3.1 The Design Objective

The objective of this research is to develop a novel collaborative continuum robot system that utilizes a mechanical lock mechanism to facilitate the connection of support continuum robots to a task-completing robot's body. This in turn will enable the combined system to achieve higher payload capacities than what either robot could achieve individ-

ually. The aim is to enable continuum robots to perform maintenance tasks on aircraft engines, such as turbine blade repairs and engine coating. Furthermore, the study aims to create a joining mechanism with an increased load bearing capacity, which can withstand axial thrust forces estimated at 235.4 N during the machining of aircraft grade aluminum using a number 6 drill bit [5]. The ultimate goal is to minimize the maximum deflection of a continuum robot to less than 1% maximum deflection to ensure the accuracy and precision of the machining process.

3.2 Conical Clutch Design Inspired Design

The first design aimed to maximize the strength of the holding mechanism. The design utilizes a Conical Clutch, a type of locking mechanism used to connect two separate moving parts [18].

The design was inspired by aluminum extrusion presses in automotive manufacturing plants. The extrusion press holds down a mold of the desired extruded aluminum's shape, and then the aluminum is fed in from the back. For this design to work, the mould assembly must be able to withstand pushing forces on the order of tons and hold the aluminum back from slipping out.

This design works in two parts; the main task-completing continuum robot will carry a cylindrical key along one of its sides, while the supporting (also referred to as helper) continuum robot will carry the lock and its supporting structure, at its end-effector. See figure 9 for a sketch of how this mechanism would work on a pair of continuum robots.

In its resting state, the locking mechanism's lock (the sliding part) will be pushed upwards, and is held up by springs placed inside of the I-beam structure. To lock a key, a cable will pull the lock down, pushing the lock against the springs, enabling the key to slide into position. Releasing the tension on the cable will result in the springs pushing the lock back into its closed position and trapping the key. See Figures 10, 11 and 12.

We can evaluate this design based on the previously defined metrics, criteria and constraints:
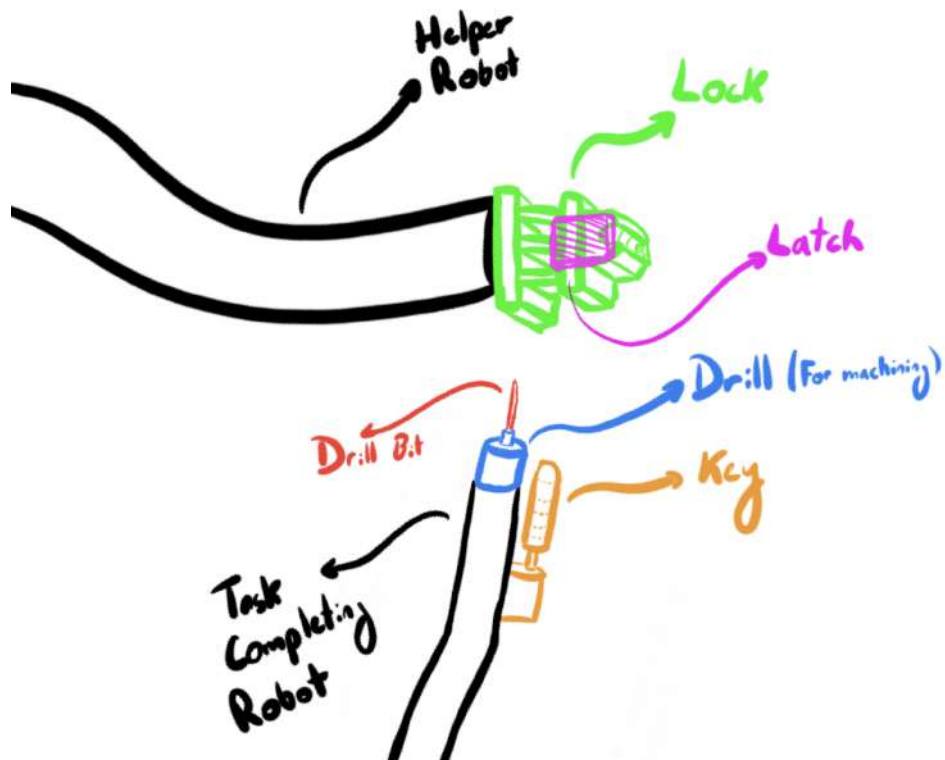
Figure 9: Conical Clutch Conceptual Design Sketch
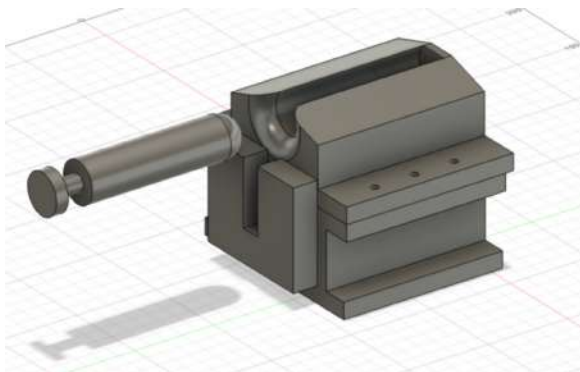
Figure 10: Conical Clutch Design Lock Isometric View (Opened Configuration).
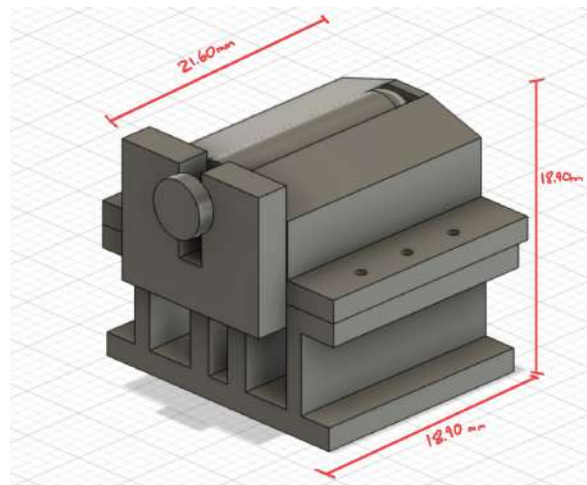
Figure 11: Conical Clutch Design Lock Isometric View (Closed Configuration)
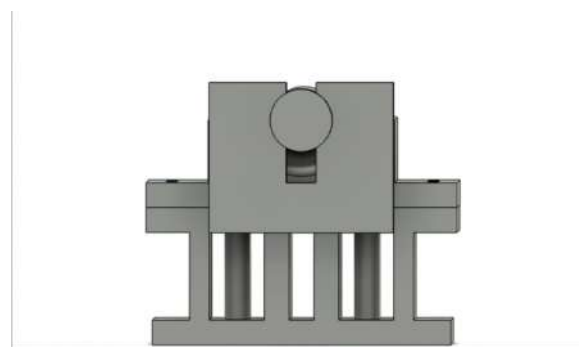
Figure 12: Conical Clutch Design Lock Elevation View (Closed Configuration)

Metrics	Evaluation	Meets Constraint
Time to Actuate the mechanism	Instantly	Yes
Time to Disengage the mechanism	Instantly	Yes
Symmetry of Design	None	No
Presence of Self-Aligning Mechanism	Yes, fillet'ed entry	N/A
Failure Load Capacity	186 N*	Yes*
Number of helper robots that can attach to a task-completing robot	1	Yes
Weight	Lock: 18.7 g Key: 5 g	N/A
Size (H, L, W) (in mm)	Lock: 18.9 x 18.9 x 21.6 Key: 4 x 20 x 4	Yes
Difference in Task-completing robot Deflection with and without mechanism	Not Tested	-
Difference in Maximum Load Capacity of Task-completing robot with and without mechanism	Not Tested	-

Table 2: Conical Clutch's Performance for the outlined metrics, criteria and constraints.

Note: * Represents simulated/estimated values.

The weight metric's evaluation was estimated using Fusion360's weight estimation feature using the Tough 2000 resin as the material as the software did not have an estimate of the Tough V5 resin. Although it is not a perfect estimate, it will serve as a reference point. The parameters used by Autodesk to estimate the resin density such as the layer thickness and how the material is cured is unknown. The value is meant to be used as a

reference.

The Failure load capacity was estimated as follows:

$$UTS = \frac{F_{UTS}}{Area} \tag{1}$$

Where UTS is the Ultimate Tensile strength of the Tough V5 Resin, 55.7 MPa [19], and Area is the cross-sectional area of the lock perpendicular to the shearing motion, estimated to be 3.34 mm^2 in Fusion360, the CAD software used to model this mechanism.

Rearranging the equation, we can find that $F_{UTS} = 186N$, which is the estimated breaking force of the mechanism. This estimate is much higher than what can be normally expected by this mechanism, as there are a multitude of factors not being taken into account such as the elasticity of the material, imperfections in the print etc. This calculation only serves as a starting off point to validate that the mechanism can withstand over 10 N of force.

Although this design incorporated a self-aligning mechanism, it does not present any useful symmetries. This would require the task completing robot and any helper robots be in a particular orientation for the mechanism to work. Circular symmetry is preferred as continuum robot disks are often circular by design, to fit into small access ports.

As no continuum robot has been built, metrics regarding the deflection and load capacity of a robot using this design could not be evaluated.

Overall, this design does not perform well as it is large, heavy, presents no useful symmetries and only permits one helper to one key. This design did however have a very high theoretical failure load capacity.

3.3 Solenoid Powered Continuum Disk Mag-lock

The next iteration of designs opted to prioritize a fault-tolerant design instead of a higher payload capacity one to achieve all criteria and constraints better than the conical clutch design. This design uses a friction clutch as a lock [18]. The design was inspired by fail-secure mag-locks.

Unlike the conical clutch design, in this design, the key is attached directly to the task-completing continuum robot's disk. This mechanism works by having the key push the latch into position, until the latch gets caught by the lock, which holds it down. The solenoid is used to open the lock far enough for the latch to be released. See Figures 13 to

18. The CAD model pictured does not include the solenoid. Figure 13 has an annotated sketch that will be useful for the rest of this document.
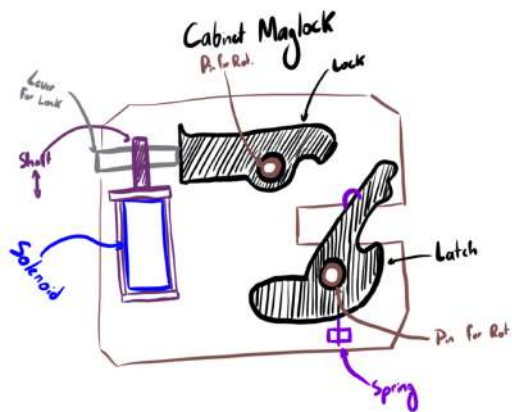
Figure 13: Continuum Disk Mag-lock Annotated Sketch.
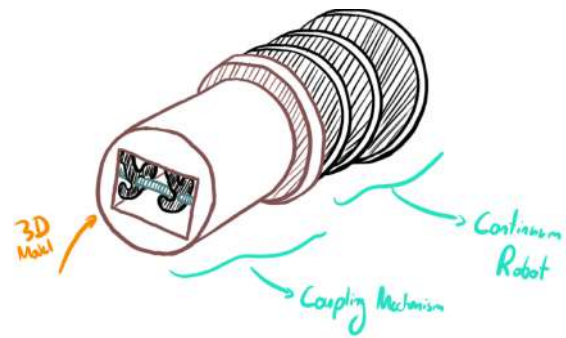
Figure 14: Continuum Disk Mag-lock Isometric View Sketch.
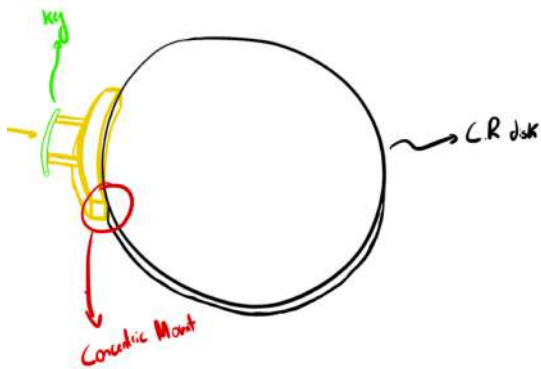
Figure 15: Continuum Disk Key Annotated Sketch.
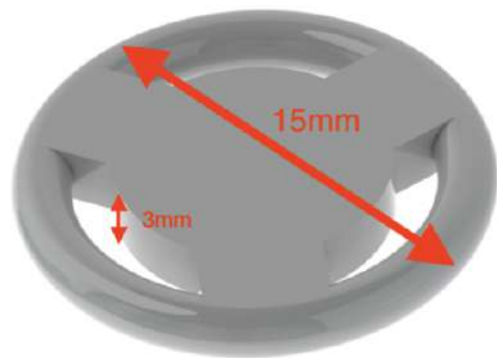
Figure 16: Continuum Disk CAD model Isometric View.
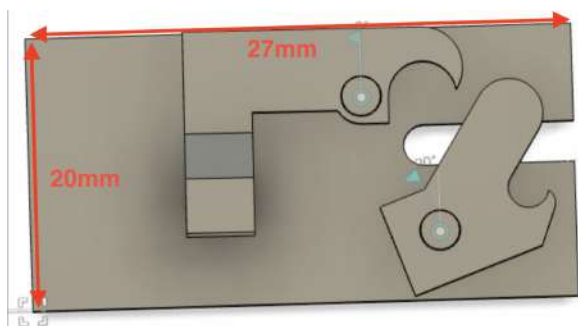
Figure 17: Continuum Disk Mag-lock Side View (Open Configuration).
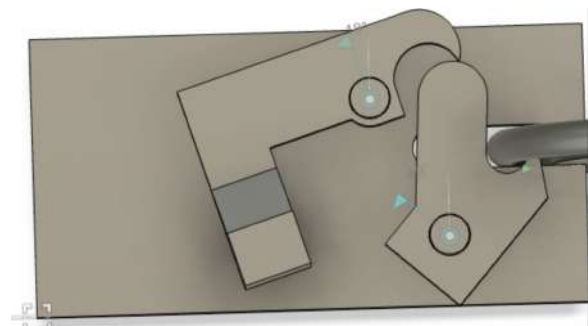
Figure 18: Continuum Disk Mag-lock Side View (Closing Configuration).

Evaluating the continuum disk mag-lock design using the aforementioned metrics, criteria and constraints:

Metrics	Evaluation	Meets Constraint
Time to Actuate the mechanism	Instantly	Yes
Time to Disengage the mechanism	Instantly	Yes
Symmetry of Design	Circular Symmetry on the Key	Yes
Presence of Self-Aligning Mechanism	None	N/A
Failure Load Capacity	142 N*	Yes*
Number of helper robots that can attach to a task-completing robot	Up to 3 per disk	Yes
Weight	Lock: 16.49 g Key: 0.717 g	N/A
Size (H, L, W) (in mm)	Lock: 20 x 27 x 6.5 Key: 0 x 0 x 0 *	Yes
Difference in Task-completing robot Deflection with and without mechanism	Not Tested	-
Difference in Maximum Load Capacity of Task-completing robot with and without mechanism	Not Tested	-

Table 3: Solenoid Powered Continuum Disk Mag-lock Performance for the outlined metrics, criteria and constraints.

Note: * Represents simulated/estimated values.

The weight is estimated through the use of Fusion360's weight estimate feature and by adding the weight of store bought parts, such as a miniature solenoid and dowel pins.

The weight of those parts were found either from datasheets from the manufacturer, or estimated using the materials' density and the parts volume.

The key itself is a continuum disk, so the weight of the key is both due to the design and a structural part of the continuum robot.

The Failure load capacity was estimated just as before using the Ultimate Tensile Strength equation, equation 1. Here, UTS is the Ultimate Tensile strength of the Tough V5 Resin, 55.7 MPa [19]. The Area is the surface area "shaved off" if the latch shears right through the lock, estimated to be 2.55 mm^2. The other failure mode possible would be of the key shearing right through the latch, but that requires a higher shearing force for this design and as such has been left out.

Rearranging equation 1, we can find that $F_{UTS} = 142N$, which is the estimated breaking force of the mechanism. This estimate is clearly an overestimate, as with this design is possible to free the key from the mechanism without breaking it apart; pulling on the key hard enough deforms the lock enough such that the latch can slip right through. After careful analysis, this behavior was in part due to not designing the geometry of the latch and lock relative to the key's position and rather having designed the key's entry after the fact. The result is that it is possible to unlock the design without exerting much force.

This proved to be a fatal flaw for this design and as such the testing did not proceed and had to be redesigned.

3.4   Servo Powered Continuum Disk Mag-lock Design

In an attempt to address the previous flaw pertaining to forcibly unlocking the mechanism, a new servo powered mechanism was designed. This design functions similarly to the Solenoid Powered Continuum Disk Mag-lock, with the exception of using a servo motor to open and close the lock.

This design would enforce the lock to stay down until the latch forcibly bends it out of shape or breaks it. The design can be observed in figures 19 to 20. The disk design remained unchanged.
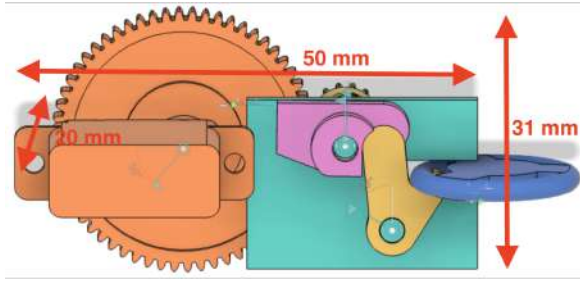
Figure 19: Servo Mag-lock CAD Front View.
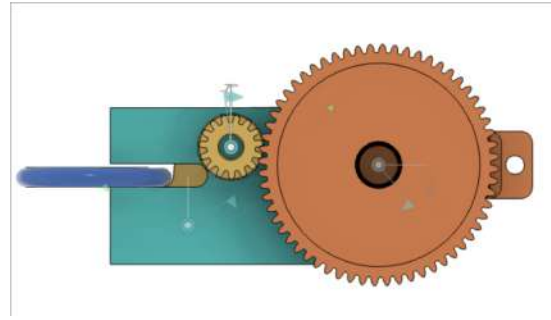
Figure 20: Servo Mag-lock CAD Back View.

Once again, evaluating this design on the metrics, criteria and constraints outlined above:

Note: * Represents simulated/estimated values.

The weight has been estimated as before; for 3D printed parts the estimates given by Fusion360's estimator using the Tough 2000 resin. The weight of off the shelf parts were found from their datasheets.

The Failure load capacity estimate is identical to that of the Solenoid powered mechanism, as the failure load is only taking into account the load that will forcibly break open the lock and free the key.

This design however suffered from its large size and complex mechanism. Given how large the design has become, it can no longer meet the size requirements, rendering this design unusable. Any redesigns made to reduce the size of the system greatly increased the complexity and weight of the system, requiring an intricate metal gear-system.

3.5 Cable Actuated Continuum Disk Mag-lock Design

To reduce overall size of the design, this current iteration of the design opted to remove the servo motor. Instead, the latch will be powered using a cable attached at its rear. In a continuum robot, this cable will run through the backbone of the robot to be pulled at the base. An additional standoff was added near the back of the mechanism, to act as a pulley to redirect the direction of the cable before pulling down the latch.

To make the mechanism close on its own, a torsional spring has also been added to the latch. The torsional spring selected produces a maximum of 0.0136 N·m of torque, selected from a pool of other similarly sized springs of various stiffness'. The spring was

Metrics	Evaluation	Meets Constraint
Time to Actuate the mechanism	Instantly	Yes
Time to Disengage the mechanism	Instantly	Yes
Symmetry of Design	Circular Symmetry on the Key	Yes
Presence of Self-Aligning Mechanism	None	N/A
Failure Load Capacity	142 N*	Yes*
Number of helper robots that can attach to a task-completing robot	Up to 3 per disk	Yes
Weight	Lock: 10.82 g Key: 0.717 g*	N/A
Size (H, L, W) (in mm)	Lock: 20 x 50 x 31 Key: 0 x 0 x 0 *	**No**
Difference in Task-completing robot Deflection with and without mechanism	Not Tested	-
Difference in Maximum Load Capacity of Task-completing robot with and without mechanism	Not Tested	-

Table 4: Servo Powered Continuum Disk Mag-lock Design Performance for the outlined metrics, criteria and constraints.

selected based on it's ability to hold the latch down on it's own and the ease of the lock to push it open.

A "step" near the bottom of the system was also added to the design, to ensure that the lock can not fall far enough to block the passage of a key.

This design also features a back-plate to hold the system together. It aims to stabilize

the various dowel pins and provide structural support for the mechanism. This modification now enables the system to operate in any orientation, as previous systems were designed to only be tested on a table.

Finally, the disk was also re-designed this iteration, this time it can accommodate up to 4 locking mechanisms at once. Holes were also made to accommodate a Nitinol backbone and Nitinol rods. See figures 21 to 24.
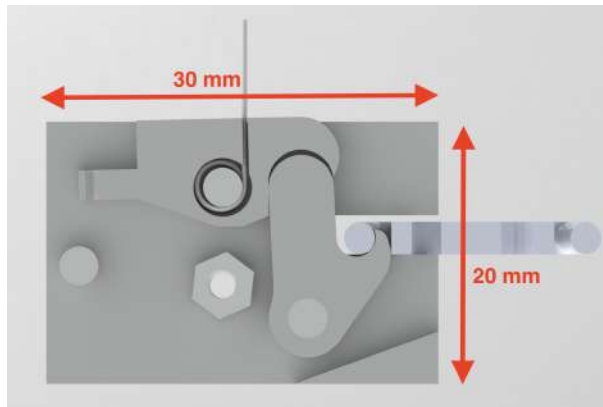
Figure 21: Cross section view of the Cable Actuated Continuum Disk Mag-lock design in it's closed configuration.
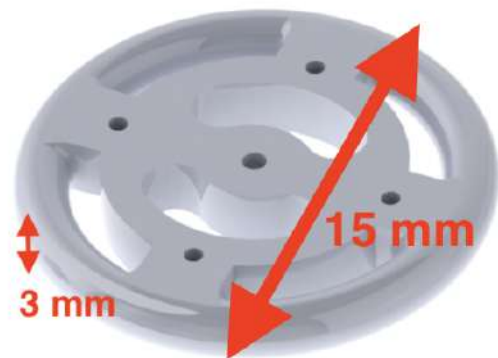
Figure 22: Continuum Disk CAD Isometric View.
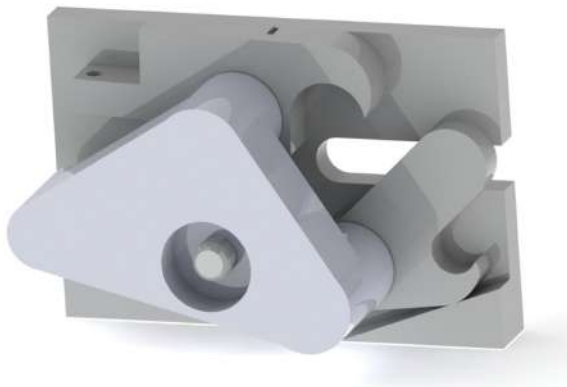
Figure 23: Isometric view of the Cable Actuated Continuum Disk Mag-lock design in its open configuration.
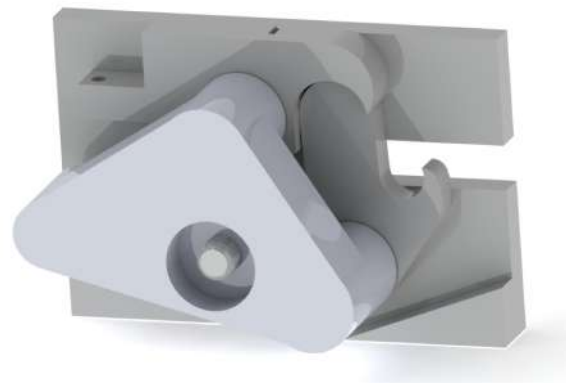
Figure 24: Isometric view of the Cable Actuated Continuum Disk Mag-lock design in its closed configuration.

Metrics	Evaluation	Meets Constraint
Time to Actuate the mechanism	Instantly	Yes
Time to Disengage the mechanism	Instantly	Yes
Symmetry of Design	Circular Symmetry on the Key	Yes
Presence of Self-Aligning Mechanism	Yes	Yes
Failure Load Capacity	298 N*	Yes*
Number of helper robots that can attach to a task-completing robot	Up to 4 per disk	Yes
Weight	Lock: 5.00 g Key: 0.48 g	N/A
Size (H, W, L) (in mm)	Lock: 20 x 30 x 12.5 Key: 0 x 0 x 0 *	Yes
Difference in Task-completing robot Deflection with and without mechanism	Not Tested	-
Difference in Maximum Load Capacity of Task-completing robot with and without mechanism	Not Tested	-

Table 5: Cable Actuated Continuum Disk Mag-lock Design Performance for the outlined metrics, criteria and constraints.

Note: * Represents simulated/estimated values.

The failure load capacity was estimated using equation 1. Here, UTS is the Ultimate Tensile strength of the Tough V5 Resin, 55.7 MPa [19]. Unlike previous calculations, this time it was found that the failure will occur at the latch, holding the key. The sheared off surface area is estimated at 5.35 mm^2. Using Equation 1 and re-arranging to find

the force associated with the ultimate tensile strength, we get that $F_{UTS} = 298N$. Once again, this is an overestimate, as it is only estimating the force required for the key to break off the latch, and not necessarily the force required for the key to bend the lock and free itself.

This design was able to be forced open by pulling on the key with moderate resistance. This time, it was because of the design of the latch not fully interfacing with the lock.

3.6   Optimized Continuum Disk Mag-lock Design

To rectify the design, the lock and latch were redesigned. The latch's shape was redesigned to fit within the lock's hole while ensuring that pulling on the key does not result in an upwards force-component and instead only towards the lock and downwards. This change is critical in ensuring that the lock does not open. Previously when pulling on the key, a small upwards force acting from the key to the latch would lead to a moment on the lock's center of rotation, opening it up. The latch was also reinforced in this design; the part that comes in contact with the disk has been reinforced and its shape now conforms to the radius of the disk, ensuring a greater contact area, increasing the shear force required to break it open.

This new design also features a newer and stiffer torsional spring, capable of producing a maximum torque of 0.0373 N·m. This change was made to increase the force required to unlock the design, in case the key is not pushed in all the way.

There is also a new self-aligning mechanism in the form of a chamfered entry, enabling easier alignment between the mechanism and key.

See Figures 25 to 28.

Figure 25: Side View of the Optimized Continuum Disk Mag-lock design.
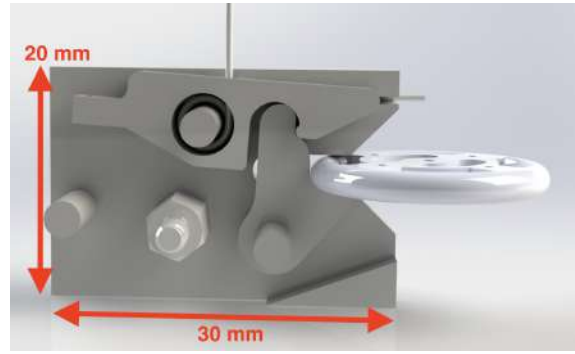
Figure 26: Side view without back-plate.
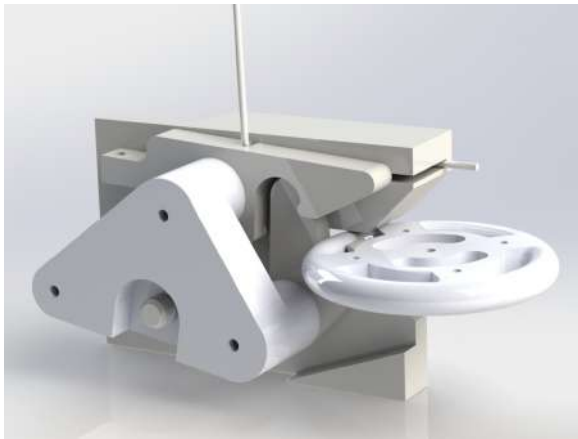
Figure 27: Isometric view.

Figure 28: Continuum Disk CAD Isometric View.

Note: * Represents simulated/estimated values.

The failure load capacity was estimated using equation 1. Here, UTS is the Ultimate Tensile strength of the Tough V5 Resin, 55.7 MPa [19]. Just like with the Cable actuated design, the failure will occur at the lock, holding the key. The shearing surface area is estimated at 6.58 mm^2. Using Equation 1 and re-arranging to find the force associated with the ultimate tensile strength, we get that $F_{UTS} = 367N$. Once again, this is an overestimate, as it is only estimating the force required for the key to break off the lock, and not necessarily the force required for the key to bend the lock and free itself.

Unlike the previous designs, when tested, this one firmly locked the key until it was released by the mechanism. As such, a modified version of the mechanism was designed to be mounted to an optics table to test it's failure load capacity empirically. See Figure 29 for the modified design. A quick test has shown that this mechanism was able to bear a 20 N load on its key, see figure 30. This test was performed by attaching a fishing line

Metrics	Evaluation	Meets Constraint
Time to Actuate the mechanism	Instantly	Yes
Time to Disengage the mechanism	Instantly	Yes
Symmetry of Design	Circular Symmetry on the Key	Yes
Presence of Self-Aligning Mechanism	Yes	Yes
Failure Load Capacity	367 N*	Yes
Number of helper robots that can attach to a task-completing robot	Up to 4 per disk	Yes
Weight	Lock: 4.12 g Key: 0.48 g*	N/A
Size (H, W, L) (in mm)	Lock: 20 x 30 x 12.5 Key: 0 x 0 x 0 *	Yes
Difference in Task-completing robot Deflection with and without mechanism	Not Tested	-
Difference in Maximum Load Capacity of Task-completing robot with and without mechanism	Not Tested	-

Table 6: Optimized Continuum Disk Mag-lock Design Performance for the outlined metrics, criteria and constraints.

from the continuum disk key to a suspended bag with 2 kg in weights. This test is not to be taken as a final result, only as a proof of concept. A proper test procedure must be developed and is discussed in the Future Work section.
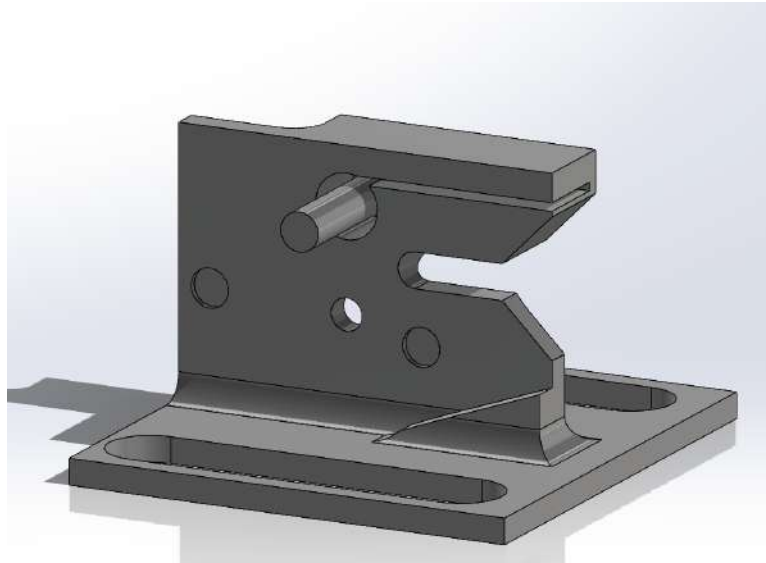
Figure 29: Mechanism modified for testing purposes.
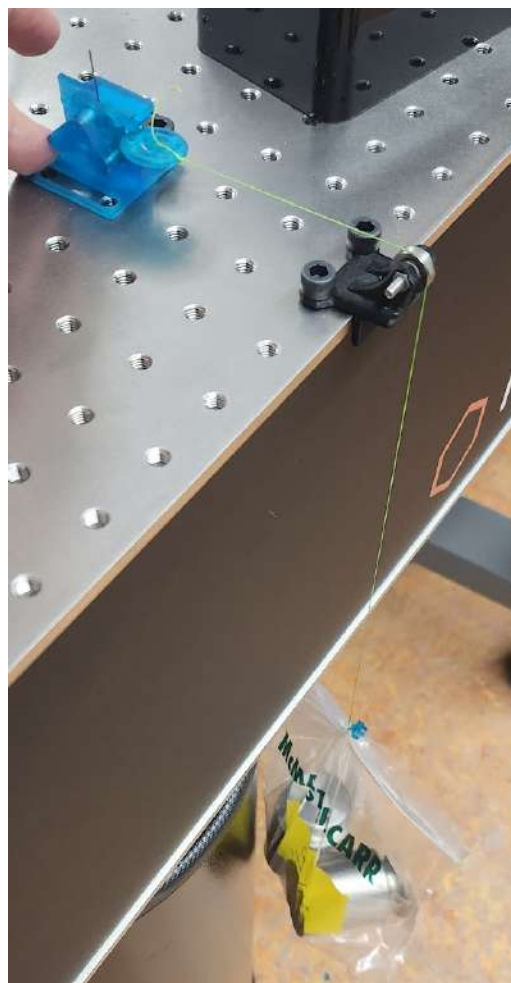
Figure 30: The Optimized Continuum Disk
Mag-lock design under a 20 N load.

3.7 Full Comparison

To put all the designs in context, table 7 compares all designs.

Metrics	Conical Clutch	Solenoid	Servo	Cable Actuated	Optimized Design
Time to Actuate the mechanism	Instantly	Instantly	Instantly	Instantly	Instantly
Time to Disengage the mechanism	Instantly	Instantly	Instantly	Instantly	Instantly
Symmetry of Design	No	Yes	Yes	Yes	Yes
Presence of Self-Aligning Mechanism	Yes	No	No	Yes	Yes
Failure Load Capacity Estimate	186 N	142 N	142 N	298 N	367 N
Number of helper robots that can attach to a task-completing robot	1	Up to 3 per disk	Up to 3 per disk	Up to 4 per disk	Up to 4 per disk
Weight	Lock: 18.7 g	Lock: 16.42	Lock: 10.82 g	Lock: 5.00 g	Lock: 4.12 g
	Key: 5 g	Key: 0.717 g	Key: 0.48 g	Key: 0.48 g	
Size (H, L, W) (in mm)	Lock: 19 x 19 x 21.6	Lock: 20 x 27 x 6.5	Lock: 20 x 31 x 50	Lock: 20 x 30 x 12.5	Lock: 20 x 30 x 12.5
	Key: 4 x 20 x 4	Key: 0 x 0 x 0	Key: 0 x 0 x 0	Key: 0 x 0 x 0	Key: 0 x 0 x 0
Difference in task-completing robot deflection with and without mechanism	Not Tested	Not Tested	Not Tested	Not Tested	Not Tested
Difference in Maximum Load Capacity of task-completing robot with and without mechanism	Not Tested	Not Tested	Not Tested	Not Tested	Not Tested

Table 7: Optimized Continuum Disk Mag-lock Design Performance for the outlined metrics, criteria and constraints.

4 Design Evaluation

4.1 Original Testing Plan

4.1.1 Failure Load Capacity

Originally, to evaluate the failure load capacity, designs will be mounted to an optics table, and using a pulley, different weights attached to the key will be suspended. The largest weight supported before the design's failure will serve as the failure load capacity of the mechanism. This will function similar to what can be observed in figure 30. See Figure 48.1 for an illustration of the test.

To be more robust, this test was instead modified to test the Failure Load Capacity at different force angles, to better replicate the conditions the mechanism would experience in non-ideal conditions. See Section 4.2 for more information about the current testing plan.

4.1.2 Deflection Tests

Originally, tests to evaluate the difference in the task-completing robot's deflection with and without the mechanism were planned.

Due to time constraints, these deflection tests were not performed. More about this in Section 8.

4.2 Testing Plan

As stated earlier, the Failure Load Capacity Test was modified to be more robust and instead replicate a wider range of conditions that the mechanism can experience when in use.

4.2.1 One DOF Testing

Initially, the idea was to measure the Failure Load Capacity of the mechanism across the "locking plane". That is the plane perpendicular to the latch. See Figure 31 for a picture of the testing mechanism.

In this initial design, the locking mechanism was positioned in the center of a semi-circle, around which a pulley can be positioned at predefined angles (0°, 22.5°, 45°, 67.5°, 90°, 112.5°, 135°, 167.5° and 180°). These angles were chosen as they are evenly distributed across the semi-circle and as such offer a good estimate of how the robot will perform when subjected to disturbances anywhere in the plane. Angles below 0° and greater than 180° are not considered as they will in fact just be pushing into the mechanism and by extension, the supporting robots. See figure 32 for a labelled picture of the mechanism (this one DOF model only concerns itself with θ). This testing method was not used to generate results, it served as the foundation for the two DOF version of this test.
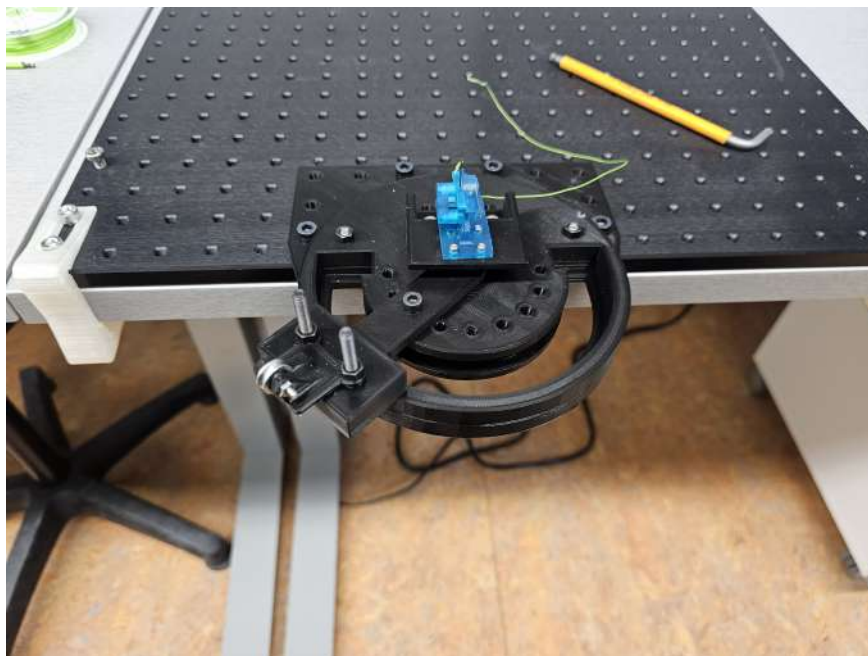
Figure 31: Picture of the 1 DOF testing mechanism.

4.2.2 Two DOF Testing

After designing the one DOF mechanism, it became apparent that these results provided by it would not be complete enough to test the viability of this locking mechanism, as realistically the two joining robots will not be perfectly parallel to one another, there are always disturbances. To make the testing more robust, the testing mechanism was improved by incorporating a secondary axis perpendicular to the locking direction in addition to the one presented in section 4.2.1.

This way, by combining both degrees of freedom, the mechanism can be tested in a

variety of scenarios and orientations more akin to its use in a cramped environment. The 2$^{\text{nd}}$ axis has predefined angles of 0°, 15°, 30° and 35°. Angles greater than 0° were chosen as this current version of the mechanism was not envisioned to support angles less than 0°. This design flaw can be easily rectified, possible solutions are explored in section 8. Angles greater than 35° are not currently possible in the design, as that is the maximum angle that the self-aligning feature supports, see figures 25 to 27 from section 3.6. See figures 32 and 33 for pictures of the testing setup.

Figure 32: Labelled image of the 2 DOF testing mechanism.
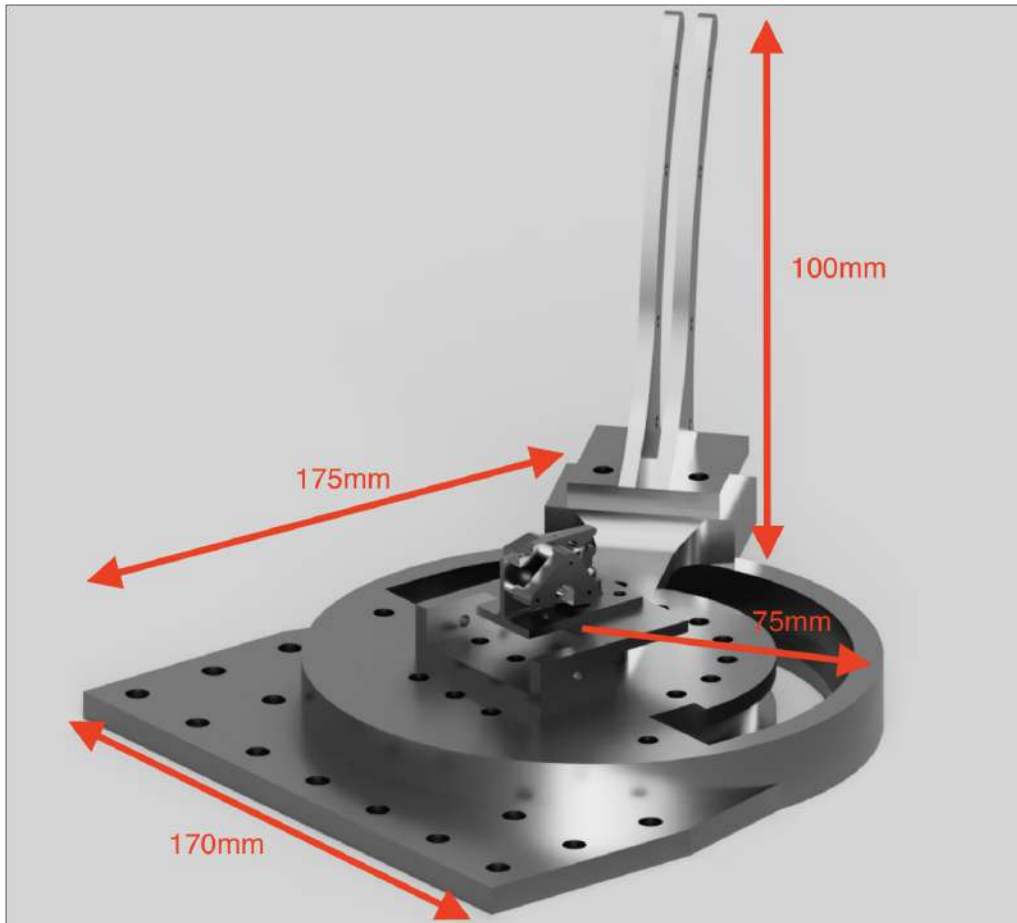
Figure 33: Render of the 2 DOF testing mechanism in CAD.

4.3 Testing Procedure

To test the mechanism, I followed the following procedure:

1. Select the desired orientation (θ and ϕ)

2. Load the mechanism with standard weights in increments of 50g and gently load the mechanism

3. Repeat Step 2 until failure

4. Swap out the latch every 4 trials, or sooner if something breaks

It is worth noting the definition of a failure, as there are three broad categories:

- **Catastrophic Failures:** These occur whenever the latch breaks. In these cases, we replace the latch with a new one, assess the damage, lower the weight of the load by 50g and try again.

36

- **Latch Openings:** These occur whenever the weights fall due to the latch opening. In this case, we make sure that no damage has occurred to the parts, and then try again after removing 50g from the load.

- **Procedural Errors:** These occur whenever the mechanism is loaded too quickly, and can either lead to a catastrophic failure or a latch opening. In this case, it is important to assess the damage (if any) and then retry with the same weight but this time ensuring to gently loading the mechanism.

5 Results and Preliminary Analysis

5.1 Test Results

First and foremost, it is worth noting that tests range from 0g to 3000g, constrained due to the weights available, and also as these were found to be safe bounds given deflection and strain estimates provided by simulations.

5.1.1 Failure Load Capacity at Constant ϕ

As a reminder, ϕ is the vertical angle, and θ is the horizontal angle in the 2 DOF testing setup. Parsing the data holding ϕ constant and varying θ, we can observe some interesting proprieties of the mechanism's design. First and foremost, across the board for all ϕ values tested, the results were not symmetric about 90°. As ϕ increases, the asymmetry of the results becomes more pronounced. For instance at $\phi = 0°$, the failure load is of 1390g (13.64N) at $\theta = 0°$, and then increases until it reaches $\theta = 67.5°$, from there it plateaus at a failure load capacity of 3000g (29.43N). The failure load capacity then goes below 3000g at $\theta = 135°$ and decreases further at $\theta = 157.5°$ and finally increases back to 3000g at $\theta = 180°$. A similar behavior can be observed when $\phi = 15°$, where the failure load capacity increases from $\theta = 0°$ to $\theta = 180°$

See Figure 34 for the graph.
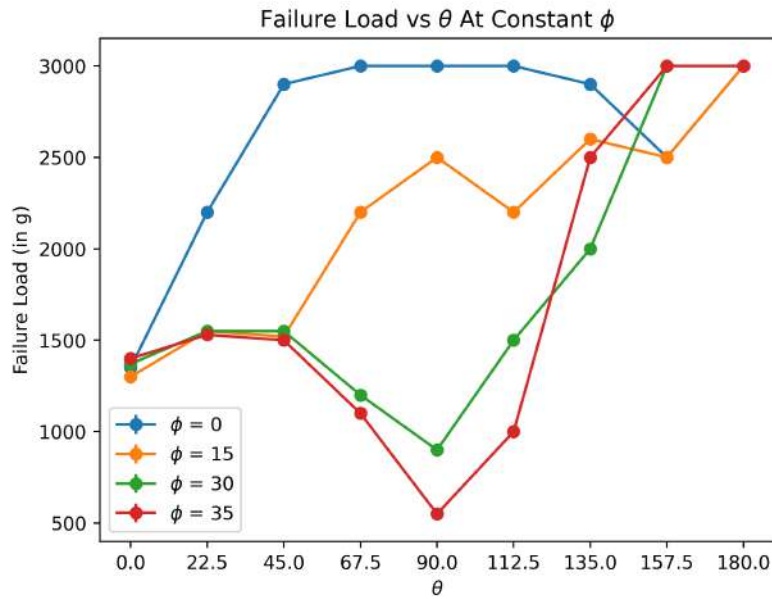
Figure 34: Failure Load Capacity of the mechanism vs θ, with ϕ is held constant.

Analysing the graph, we can see that the θ providing the highest failure load capacity varies as a function of ϕ, but in general $\theta = 180°$ provides a high failure load capacity. This is due to the nature of the design; when $\theta = 180°$, the latch has 2 points of contact with the design's "back-plate", one on top of the disk and one below. This results in the load being distributed across a greater surface area and by result a higher payload capacity.

Likewise, there seems to be some correlation between the lowest failure load capacity and ϕ; for $\phi \leq 15°$ the lowest failure load capacity is at $\theta = 0°$. This is to be expected as at $\theta = 0°$, the latch is not being held back from being deformed from the side. When analysing the used latches after tests at $\theta = 0°$, latches have been found to be warped towards the direction of the force. After being warped, the disk can slip through the crack and free itself. On the other hand, at $\phi \geq 30°$, there is a dip in the maximum failure load capacity around $\theta = 90°$. In circumstances where $\phi \geq 30°$, it makes sense for the design to behave poorly when $\theta = 90°$ as the force has a vertical component that is great enough to push open the latch enough for the disk to pull free through the crack.

5.1.2 Failure Load Capacity at Constant θ

Next, working with the data and plotting the relationship between the Failure Load Capacity versus ϕ and holding θ constant results in graphs that reveal the optimal θ value for a given ϕ.

When analyzing the graph, we can observe that for $\theta leq 112.5°$, the trend is that as ϕ increases, the load capacity decreases. This makes sense, as the expectation is that a larger ϕ results in the lock being pushed open. For $135° \leq \theta < 180°$, there seems to be a positive correlation between the failure load capacity and ϕ. This makes sense, as in these circumstances, the latch has 2 points of contact with the design's "back-plate", and any vertical force components due to ϕ are counteracted by the back-plate's slot for the disk. This results in higher ϕ values having higher failure load capacities, as now less forces are acting upon the locking mechanism itself. At $\theta = 180°$, the failure load capacity is maximum and constant, which is due to the fact that for all ϕ values, the latch is pushes against the back-plate and it bears the full load.

See Figure 35 for the graph.
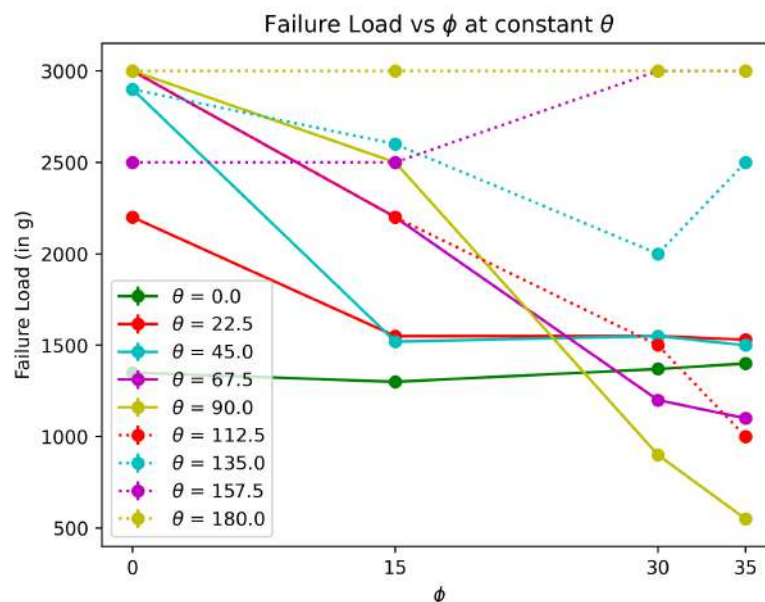
Figure 35: Failure Load Capacity of the mechanism vs ϕ, with θ is held constant

5.1.3 Force Vector Graphs

To better visualize and understand the results obtained, they have also been plotted in "vector form", where each vector represents the direction and magnitude for the Failure Load Capacity, in Newtons. By holding ϕ constant, we can better understand how θ impacts the resulting magnitude of the forces. The asymmetries alluded to above can easily be seen in this format. These graphs are meant purely for understanding the trends visually, rather than be used for empirical measurements; as such the x and y axis labels have been removed to reduce any confusion and a scale has been inserted to help understand what a difference in scale entails. See figures 36 for the graphs.
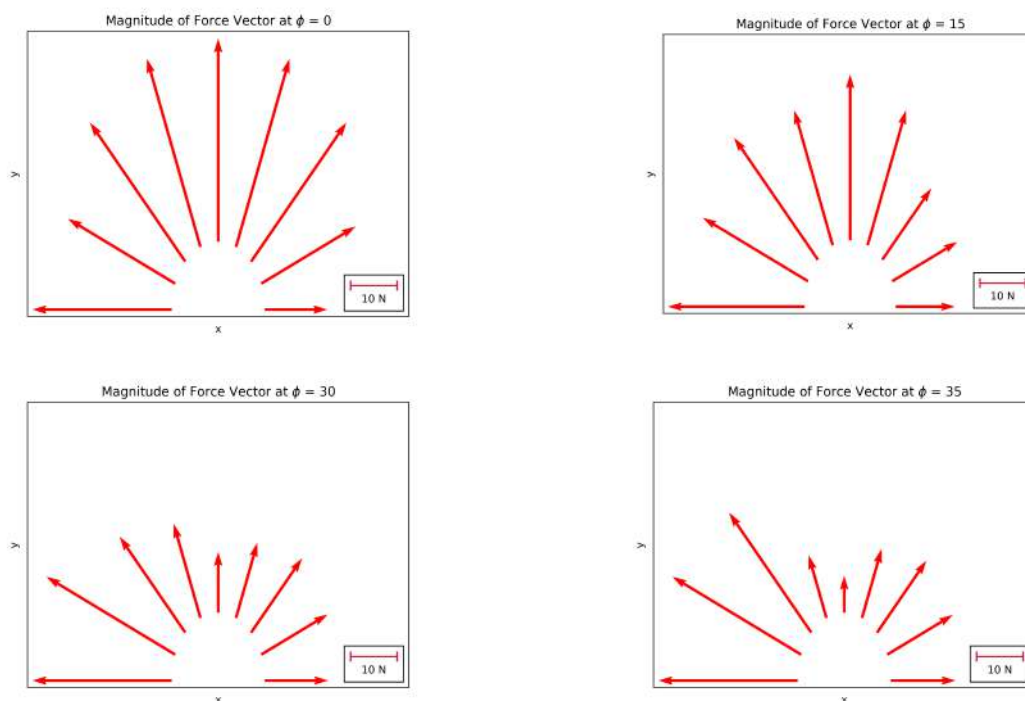
Figure 36: Force Vector graphs at different tranches of ϕ. θ is defined as the angle between the x-axis to a corresponding arrow, increasing in a counter-clockwise direction

5.2 Finite Element Analysis

To validate the results from the experiment, CAD simulations were performed in Solid-Works. These simulations used SolidWorks' Static load simulation model, with a point load of 30 N at the location where the disk would be pulling on the latch. In the interest of generality, these simulations were performed only in the axis perpendicular to the

latch, where the latch and the key would normally connect.

To perform these simulations, a custom material was created in SolidWorks with the physical properties of the Tough V5 resin used in the real models [19]. The post cured material proprieties were used, as all prints were cured before being tested. See figure 37 for the material properties used.

Material Properties Data

	METRIC[1]	
	Green[2]	Post-Cured[3]
Mechanical Properties		
Ultimate Tensile Strength	34.7 MPa	55.7 MPa
Tensile Modulus	1.7 GPa	2.7 GPa
Elongation at Break	42 %	24 %
Flexural Strength at 5% Strain	20.8 MPa	60.6 MPa
Flexural Modulus	0.6 GPa	1.6 GPa
Notched IZOD	32.6 J/m	38 J/m

Figure 37: Material properties of Tough V5 [19]

5.2.1 Latch and Lock Simulation

To perform the simulation on the latch, the shaft-hole around which the latch rotates by and the part of the connection interface between the latch and lock are made fixed. This implicitly assumes that these two components of the latch will always be at the same location, regardless of the deformation, as there are parts constraining them. A 30N load is applied to the tip of the latch, at the location where the continuum disk (the key) would be pulling on the latch. From the stress simulation results, from figure 38, it is apparent that there is an anticipated stress of 37.2 MPa near the base of the latch's "tooth", which is nearing the Ultimate Tensile Strength (UTS) of Tough V5, of 55.7 MPa [19]. As stated earlier during the design process, the UTS is the maximum stress a material can take before it fails catastrophically.

41

In addition to the stress simulation, the expected deflection (strain) was also simulated. Under the 30N load, the tip of the latch was expected to undergo a deflection of up to 0.18mm. See figure 39 for the strain simulation results.
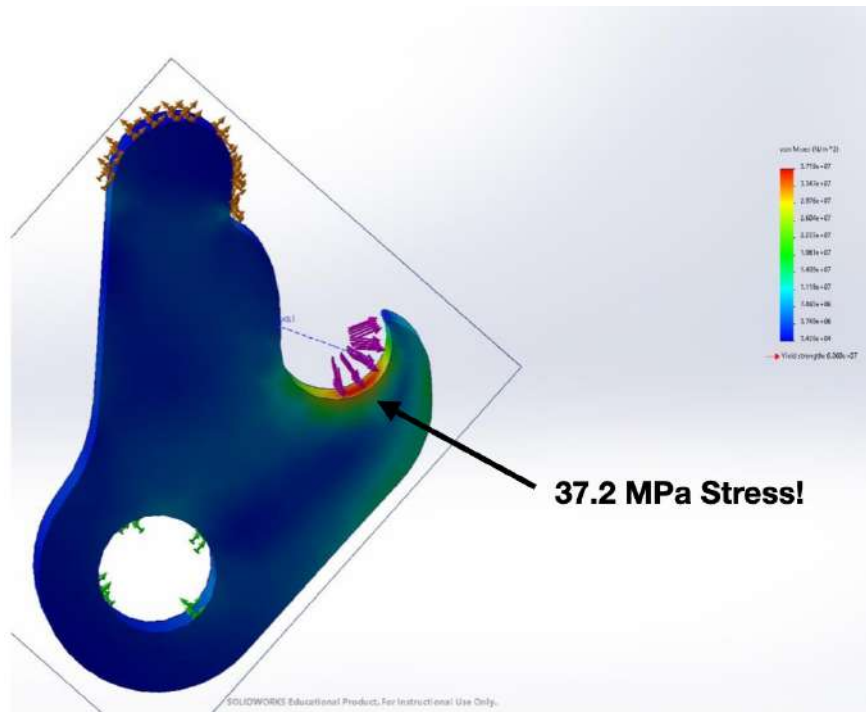
Figure 38: Stress experienced by the latch under a 30N load.
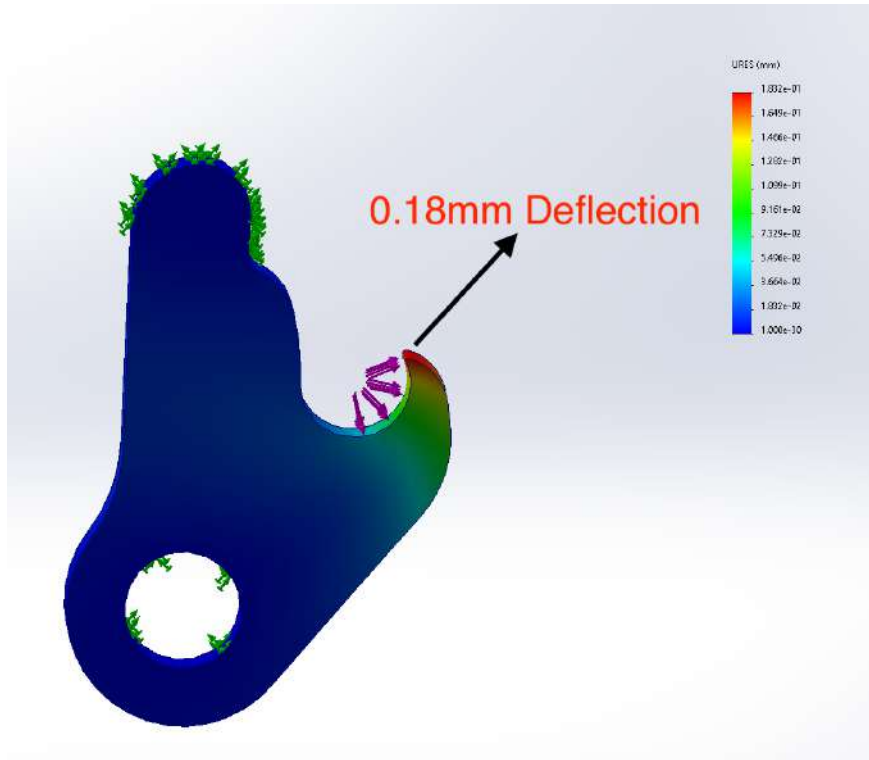
Figure 39: Deflection experienced by the latch under a 30N load.

Next, the lock was also simulated similarly. To perform simulations akin to the conditions the lock would be exposed to, the hole in which the spring attaches to the lock was set to be fixed, as it is the lock's only "grounding feature" in the full system. Also, the 30 N load used to emulate the forces the latch will be putting on the lock is applied to the contact-patch between the latch and the lock. Under this direct load, the lock experiences a peak stress of 53.45 MPa, which is very close to the UTS of Tough V5 [19]. See figure 40 for the simulation's results. The lock has also been simulated to experience a strain of 0.7mm, see figure 41 for the results.
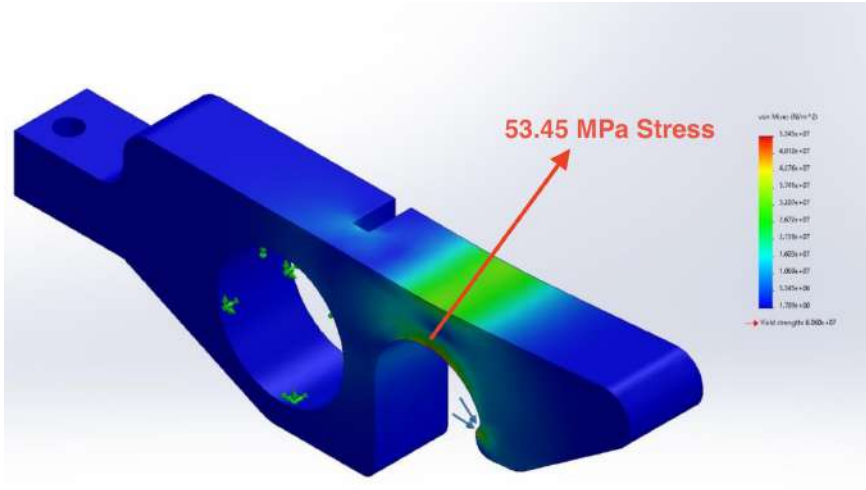
Figure 40: Stress experienced by the lock under a 30N load
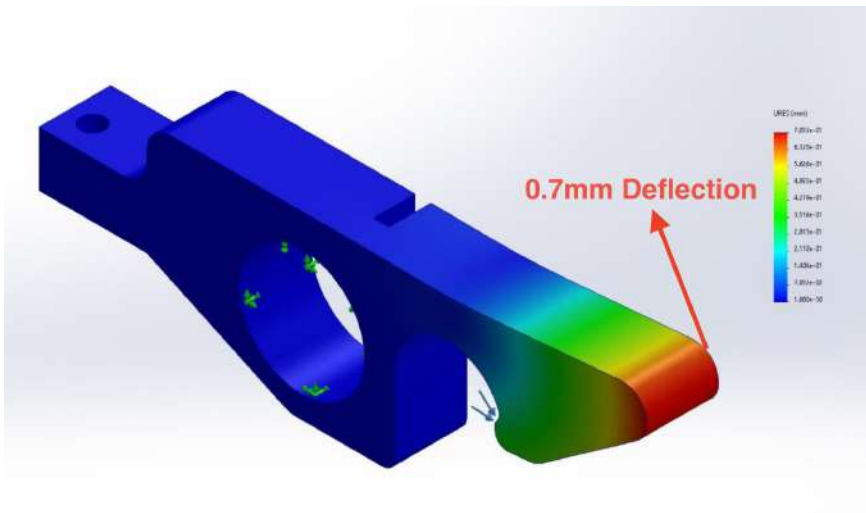
Figure 41: Deflection experienced by the lock under a 30N load.

5.2.2 Full System Simulation

Given that the mechanism is comprised of more than just the individual latch and lock, a full system simulation was also performed. As before, the system was subjected to a 30 N load at the latch, which is where the disk would attach itself to the mechanism. The back of the mechanism, where a continuum robot would attach the mechanism to one of its disks, was chosen to be fixed. The spring was simulated using a pin with a rotational stiffness of 0.03 N · m per degree, which simulates the torsional spring used with high fidelity at small angles.

When evaluating the stresses in the full system under a 30 N load at the latch, there

is a peak stress of 42.34 MPa at the latch, which is higher than what was anticipated when simulating the latch on its own, while there is a reduced amount of stress at the lock compared to it being loaded with 30 N of force directly. This is due to the fact that the lock is attached further from the axis of rotation of the latch than the location of the 30N load, it stands to reason that the force would also be proportionally smaller, as it has a larger moment arm. See figure 42 for a rendering of the stress on the system.

Likewise, when evaluating the deflection under load, the latch experiences a higher deflection of 0.7mm at its tip, which is greater than the 0.18mm from before, while the lock experiences a reduced overall strain. This also makes sense, as the latch was simulated to be fixed at its connection point with the lock, which is not the case in the real system where the lock can actually open and close a bit. See figure 43 for the results.
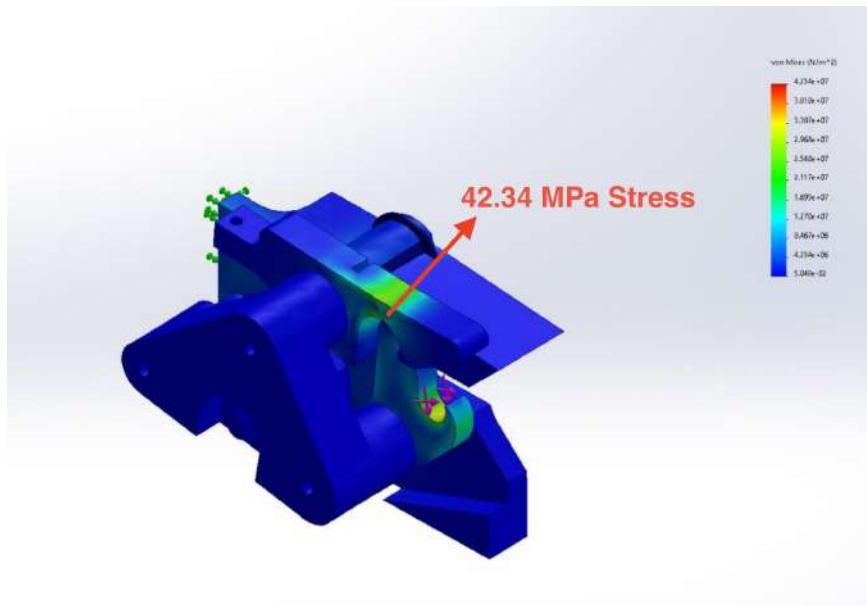
Figure 42: Stress experienced by the system under a 30N load
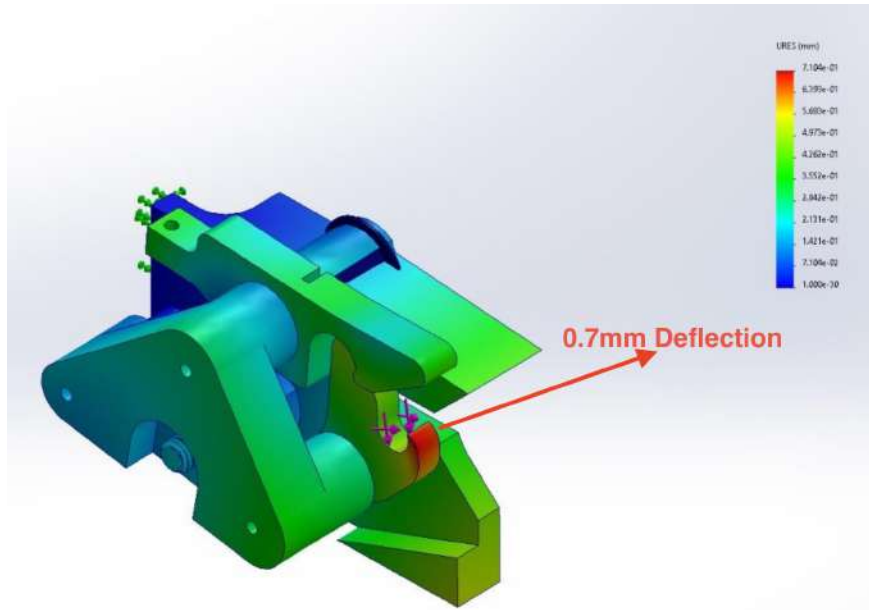
Figure 43: Deflection experienced by the system under a 30N load.

6 Analysis and Discussion

6.1 Expected Failure Loads vs Simulation

When analyzing the results from the stress simulation from the latch, we can observe that the strain in the full system is estimated to reach 42.34 MPa. It is worth noting the location at which this stress occurs; right at the bottom of the spot where the key (the continuum disk) is supposed to enter. When testing the design, fractures that result into catastrophic failures tend to propagate from the "tooth" that attaches to the key. See figure 44 for a picture of some of the failed latches.

Figure 44: Samples of failed latches and failed disks.

This discrepancy is due to the fact that the loads exerted from the disk are not uniformly applied to that region of the latch, but instead are concentrated more in the center of the part. This is due to the fact that the radius of the disk's outer ring is smaller than that of the hole present in the latch, which in turn results in the disk applying its force on one point. The design was chosen such that the disk can fit within the latch and not prohibit the locking mechanism from actuating. Other factors such as the 3D printed

parts not being fully cured can contribute to worse material properties, such as a lower Ultimate Tensile Strength, may have contributed to lower overall failure load capacities then anticipated.

The disk failures in figure 44 occurred due to procedural errors, where the weights were dropped too quickly. It is worth noting that this disk design has been optimized for this specific test procedure, and is weaker than the proposed disk design (due to having less spokes supporting the outer ring). This spoke-less design was selected to ensure that no spokes can interfere with the cable from the disk to the weight, for any θ value.

The simulation's deflection estimates were critical in understanding why the disk would free itself from the mechanism without breaking anything. Given that the latch deflects up to 0.7mm under a 30N load, we can infer that the latch would deflect, just enough for the disk to squeeze through.

7   Design Review

7.1   Design Objectives

Reviewing the design's adherence to the goals, we can generate table 8.

The final design meets most requirements, except for the length aspect of the size requirement, being 30mm long instead of 20mm. The height, width and length were computed as the total effective height, not the total height of the design as a significant portion of the mechanisms' current height is due to the table-mounting fixture. See figure 45 for an illustration of the effective height.

The initially calculated estimates of the total failure load capacity were an order of magnitude lower than the estimates, as the estimates did not account for elastic deformation of the parts, imperfections in the manufacturing process and used assumed a linear shear plane as the direction of the fractures' propagation. These simplifying assumptions made it possible to get an estimate of the relative failure load capacities of the designs

The estimates where however correct in predicting the design's failure mechanism and its weight estimate.

Metrics	Evaluation	Meets Constraint
Time to Actuate the mechanism	Instantly	Yes
Time to Disengage the mechanism	Instantly	Yes
Symmetry of Design	Circular Symmetry on the Key	Yes
Presence of Self-Aligning Mechanism	Yes	Yes
Failure Load Capacity at $\phi = 0°, \theta = 90°$	29.43N	Yes
Number of helper robots that can attach to a task-completing robot	Up to 4 per disk	Yes
Weight	Lock: 4.12 g Key: 0.48 g*	N/A
Size (H, L, W) (in mm)	Lock: 15.53 x 30 x 12.5 Key: 0 x 0 x 0 *	No*
Difference in Task-completing robot Deflection with and without mechanism	Not Tested	-
Difference in Maximum Load Capacity of Task-completing robot with and without mechanism	Not Tested	-

Table 8: Evaluation of the final design's adherence to the metrics, criteria and constraints

8 Future Work

Although the results from this thesis are not ready to be used in aircraft maintenance quite yet, a few modifications can make this design meet the size and load requirements.
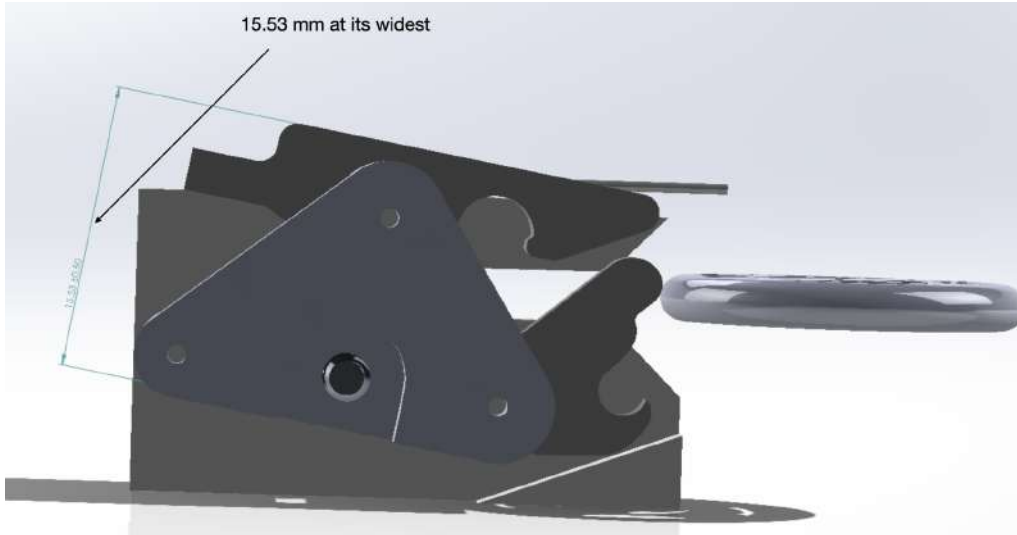
Figure 45: Effective height of the mechanism

8.1 Enhancements

For instance, shaving the mechanism' design by 0.53mm will enable the design to meet the size requirement, and can be done without impacting the failure load capacity; the mechanism's front plate (the triangle shape) is not load bearing and contributes to most of this 0.53mm. Another 0.1mm can be accounted for by choosing the "locked configuration" of the mechanism be the default, and then unlocking it before using the mechanism.

In addition to this, using a different material than Tough V5 with better material properties (higher modulus of elasticity and higher Ultimate Tensile Strength) will in turn result in a much higher payload capacity for the same design. Examples of such materials include Aluminum 7075-T6, which is a bit more dense than Aluminum 6061 ($2.81 \frac{g}{cm^3}$ vs $2.70 \frac{g}{cm^3}$) but offers an Ultimate Tensile Strength of 570 MPa, over 10x higher than Tough V5[19]. See figures 46 and 47 for simulations of the same mechanism, under 300 N of load, this time made up of Aluminum 7075-T6.
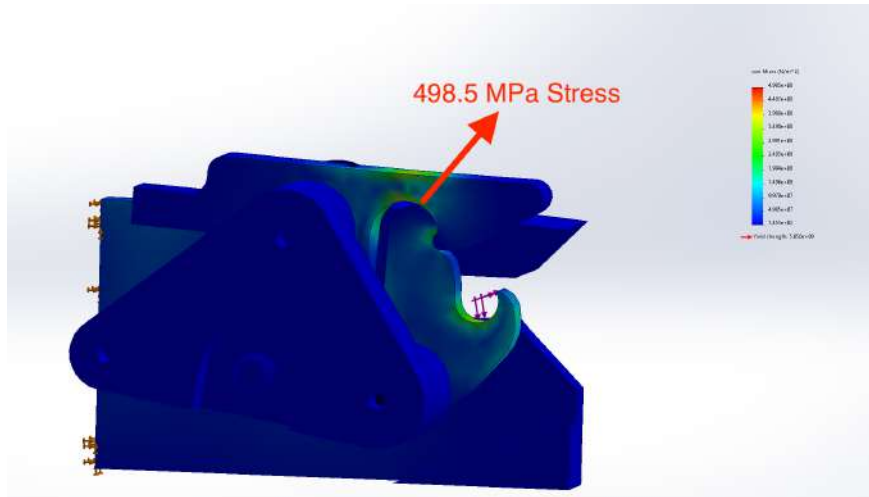
Figure 46: Stress experienced by the system under a 300N load when designed in Aluminum 7075-T6
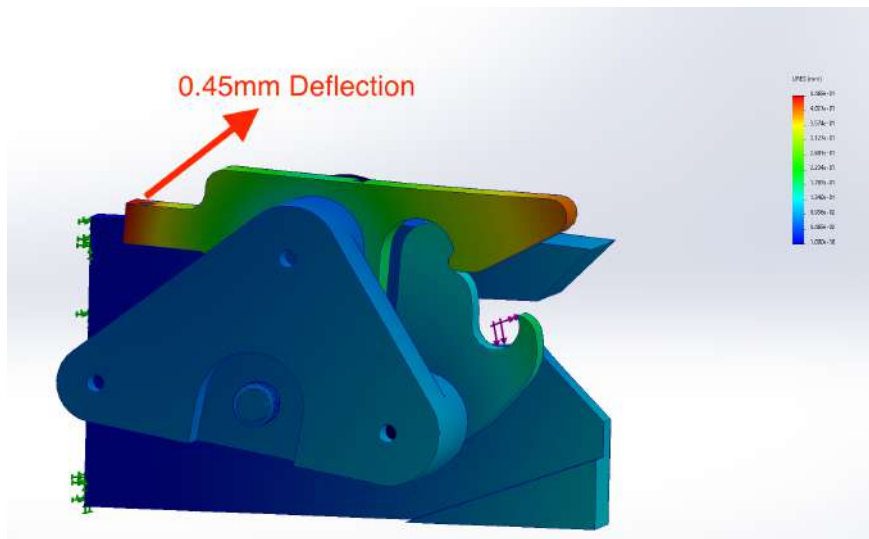
Figure 47: Deflection experienced by the system under a 300N load when designed in Aluminum 7075-T6.

Next, the design's payload capacity was asymmetric and had an axis noticeably weaker than the other, to remediate this a redesign of the front plate (the triangle part) is in order. Making it a flat plate that's parallel to the back-plate will result in higher payload capacities when $\theta 90°$. In addition to this, reinforcing the lock will also enable the design to reach higher failure load capacities. As it is the first to reach strains near the material's Ultimate Tensile Strength when loaded.

8.2   The Continuum Robots

After completing these enhancements, designing a set of continuum robots (the task completing robot and the helper) will be required. Looking into designing these robots as rod-driven continuum robots and implementing robot stiffening techniques will enable the robots to deflect less on their own.

8.3   Further Testing

To ensure the design works, validation through the use of a pair of continuum robots is necessary. Tests such as those highlighted in Section 4.1.

These tests entail having a pair of continuum robots 300 mm in length each, one task-completing, the other a helper robot, and evaluating the deflection of both robots carrying a 100g load at their tips, with and without the joining mechanism, and finally the deflection of the combined system while carrying 100g of load.

This test would be repeated twice, in two different configurations. The first configuration has the helper robot be suspended on top of the task completing robot, whereas the second configuration have both robots in the same plane. In both configurations, the robots are perpendicular to each other such that the mechanism can be in full contact. See figures 48.2 and 48.3 to see illustrations for how these tests would have been performed.
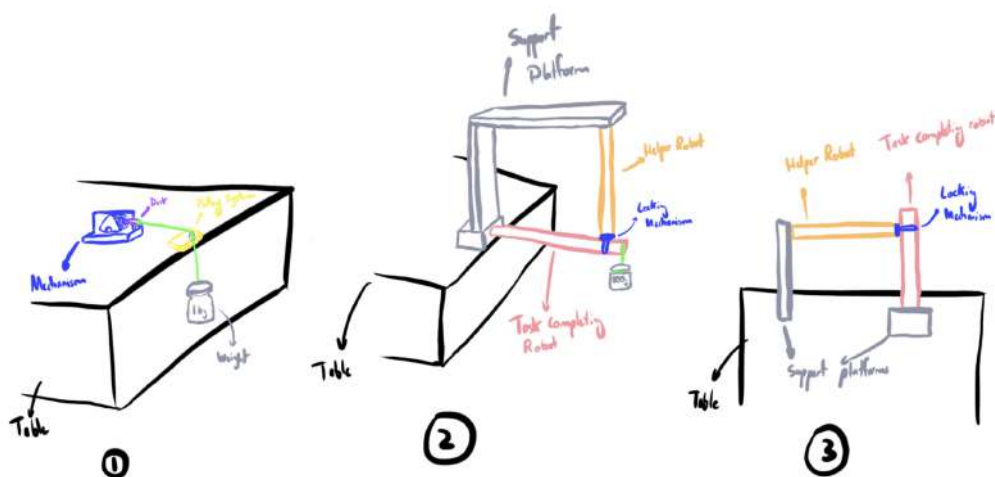

Figure 48: Sketch of the proposed tests

Following these tests, trying the mechanism in a mock aircraft maintenance scenario

is a must, as it will serve as validation for the use of this mechanism. Examples of such tests can include: performing an inspection task to find defects, such as grinding metal for a bore-bending tasks like Dong et al. have done [9].

9   Conclusion

This thesis' objective was to design a novel mechanical locking mechanism to enable support continuum robots to join a task-completing robot to increase the system's overall payload capacity. This increased payload capacity was aimed to enable the system to perform aircraft maintenance tasks, such as machining aircraft grade aluminum with a number 6 drill bit, grinding metal from turbine blades, performing flame coating repairs to the and performing safety inspection. Of these tasks, machining aircraft grade aluminum with a number 6 drill bit is the most force-intensive, requiring the system to withstand axial thrust forces estimated at 235.4 N [5]. This mechanism would need to fit within access ports of aircraft engines, requiring the individual continuum robots have a maximum overall diameter of 15mm. Finally, the system should deflect as little as possible when utilizing this mechanism.

This work aims to enable continuum robots to be used as a viable solution in untapped fields, such as aircraft maintenance. The use of continuum robots in aircraft maintenance will be complicit in reducing the overall downtime and costs associated with jet-engine maintenance thereby enabling more frequent inspection and maintenance of said engines.

As stated earlier, this mechanism was only able to withstand a maximum loading force of 29.43N before the stresses grow too great. This design is also 15.53mm thick when stripped to its smallest possible configuration, which is larger than the 15mm requirement. Finally, this design was not tested on a real pair of continuum robots. Overall, this design is not ready to be used in such an application as is, but by implementing some of the aforementioned improvements, this design can be used to accomplish this thesis' initial goal. The developed mechanism is currently capable of withstanding loads of up to 29.3N, whereas a change of materials will permit this same design to meet and exceed the 235.4N axial load requirement imposed by machining aircraft grade aluminum.

10   Bibliography

References

[1] T. -D. Nguyen and J. Burgner-Kahrs, "A tendon-driven continuum robot with extensible sections," 2015 IEEE/RSJ International Conference on Intelligent Robots and Systems (IROS), 2015, pp. 2130-2135, doi: 10.1109/IROS.2015.7353661.

[2] J. Burgner-Kahrs, D. C. Rucker, and H. Choset, "Continuum Robots for Medical Applications: A Survey," IEEE Transactions on Robotics, vol. 31, no. 6, pp. 1261–1280, 2015.

[3] P. Dupont, N. Simaan, H. Choset, and C. Rucker, "Continuum Robots for Medical Interventions," Proceedings of the IEEE, pp. 1–24, 2022.

[4] M. Russo, N. Sriratanasak, W. Ba, X. Dong, A. Mohammad and D. Axinte, "Cooperative Continuum Robots: Enhancing Individual Continuum Arms by Reconfiguring Into a Parallel Manipulator," in IEEE Robotics and Automation Letters, vol. 7, no. 2, pp. 1558-1565, April 2022, doi: 10.1109/LRA.2021.3139371.

[5] P. Kishore Kumar, Dr. K. Kishore, Prof. P. Laxminarayana, 2013, Prediction Of Thrust Force And Torque In Drilling On Aluminum 6061-T6 Alloy, INTERNATIONAL JOURNAL OF ENGINEERING RESEARCH & TECHNOLOGY (IJERT) Volume 02, Issue 03 (March 2013)

[6] D. Alatorre et al., "Teleoperated, In Situ Repair of an Aeroengine: Overcoming the Internet Latency Hurdle," IEEE Robot. Autom. Mag., vol. 26, no. 1, pp. 10–20, 2019, doi: 10.1109/MRA.2018.2881977

[7] W. Ba, X. Dong, A. Mohammad, M. Wang, D. Axinte, and A. Norton, "Design and Validation of a Novel Fuzzy-Logic-Based Static Feedback Controller for Tendon-Driven Continuum Robots," IEEE/ASME Trans. Mechatronics, vol. 26, no. 6, pp. 3010–3021, 2021.

[8] X. Dong, D. Axinte, D. Palmer, S. Cobos, M. Raffles, A. Rabani, and J. Kell, "Development of a slender continuum robotic system or on-wing inspection/repair

of gas turbine engines," Robotics and Computer-Integrated Manufacturing, vol. 44, pp.218–229, 2017.

[9] X. Dong, D. Palmer, D. Axinte, and J. Kell, "In-situ repair/maintenance with a continuum robotic machine tool in confined space," Journal of Manufacturing Processes, vol. 38, pp. 313–318, 2019

[10] M. Russo, S. M. Sadati, X. Dong, A. Mohammad, I. D. Walker, C. Bergeles, K. Xu, and D. A. Axinte, "Continuum robots: An overview," Advanced Intelligent Systems, p. 2200367, 2023.

[11] X. Dong et al., "Continuum Robots Collaborate for Safe Manipulation of High-Temperature Flame to Enable Repairs in Challenging Environments," in IEEE/ASME Transactions on Mechatronics, vol. 27, no. 5, pp. 4217-4220, Oct. 2022, doi: 10.1109/TMECH.2021.3138222.

[12] K. Nuelle, T. Sterneck, S. Lilge, D. Xiong, J. Burgner-Kahrs, and T. Ortmaier, "Modeling, calibration, and evaluation of a tendon-actuated planar parallel continuum robot," IEEE Robotics and Automation Letters, vol. 5, no. 4, pp. 5811–5818, Oct. 2020.

[13] G. Boettcher, S. Lilge, and J. Burgner-Kahrs, "Design of a reconfigurable parallel continuum robot with tendon-actuated kinematic chains," IEEE Robotics and Automation Letters, vol. 6, no. 2, pp. 1272–1279, Apr. 2021.

[14] C. Yang, S. Geng, I. Walker, D. T. Branson, J. Liu, J. S. Dai, and R. Kang, "Geometric constraint-based modeling and analysis of a novel continuum robot with Shape Memory Alloy initiated variable stiffness," The International Journal of Robotics Research, vol. 39, no. 14, pp. 1620–1634, 2020.

[15] C. Yang, S. Geng, I. Walker, D. T. Branson, J. Liu, J. S. Dai, and R. Kang, "Geometric constraint-based modeling and analysis of a novel continuum robot with Shape Memory Alloy initiated variable stiffness," The International Journal of Robotics Research, vol. 39, no. 14, pp. 1620–1634, 2020.

[16] M. Langer, E. Amanov, and J. Burgner-Kahrs, "Stiffening sheaths for continuum robots," Soft Robotics, vol. 5, no. 3, pp. 291–303, 2018

[17] Y. Li, T. Ren, Y. Chen, M. Z. Q. Chen, and S. Member, "A Variable Stiffness Soft Continuum Robot Based on Pre-charged Air, Particle Jamming, and Origami," pp. 5869–5875, 2020.

[18] R. W. Messler, Integral mechanical attachment a resurgence of the oldest method of joining. Butterworth-Heinemann, 2006.

[19] "Tough V5 Datasheet." Formlabs. Jan 26 2018. Available: https://formlabs-media.formlabs.comdatasheetsTough_Technical.pdf. [Accessed: 14-Jan-2023].

Appendices

A   Appendix A: Experimental Data

Side	Theta (deg)	Phi (deg)	Latch: Extended
	(right most = 0)	(bottom = 0)	
	Theta (deg)	**Phi (deg)**	**Failure Load (g)**
Left	0	0	1350
		15	1300
		30	1370
		35	1400
	22.5	0	2200
		15	1550
		30	1550
		35	1530
	45	0	2900
		15	1520
		30	1550
		35	1500
	67.5	0	3000
		15	2200
		30	1200
		35	1100
Center	90	0	3000
		15	2500
		30	900
		35	550
Right	112.5	0	3000
		15	2200
		30	1500
		35	1000
	135	0	2900
		15	2600
		30	2000
		35	2500
	157.5	0	2500
		15	2500
		30	3000
		35	3000
	180	0	3000
		15	3000
		30	3000
		35	3000

B   Appendix B: Latch FEA Simulation Report
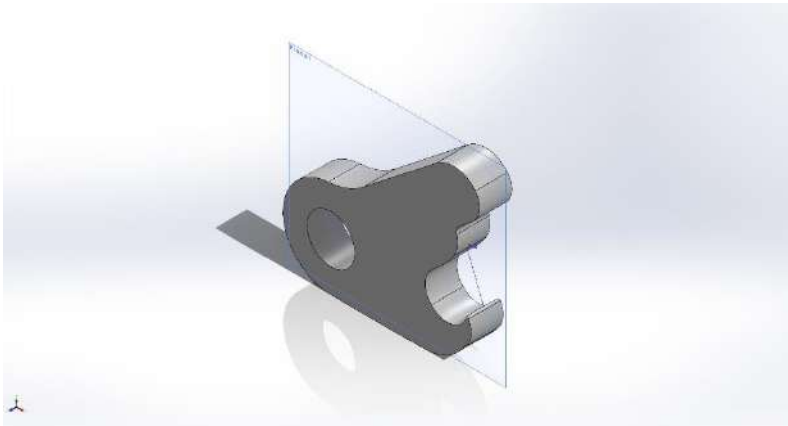
Simulation of Latch Plus Plus

Date: April 11, 2023
Designer: Ryan Zazo
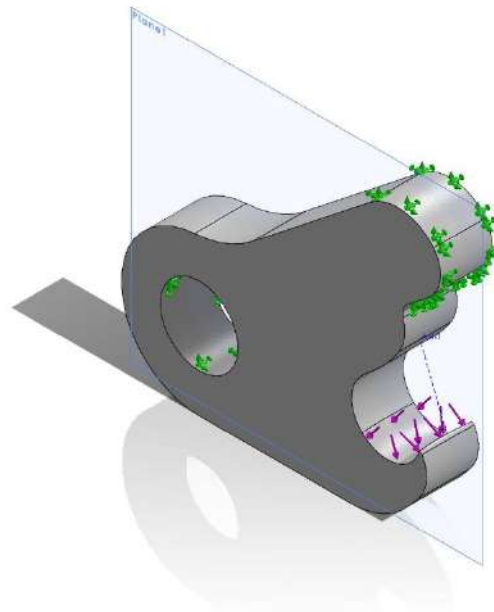**Study name:** Static 1
Analysis type: Static

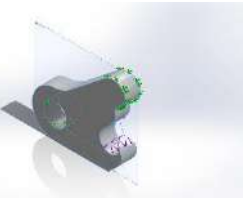## Table of Contents

Description

No Data

Assumptions

Model Information

Model name: Latch PlusPlus
Current Configuration: Default

Solid Bodies

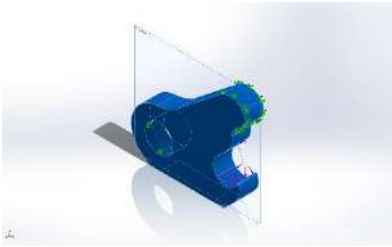| Document Name and Reference	Treated As	Volumetric Properties	Document Path/Date Modified
Fillet10	Solid Body	**Mass:0.000171591 kg Volume:1.42992e-07 m^3 Density:1,200 kg/m^3 Weight:0.00168159 N**	**C:\Users\Ryan\OneDrive - University of Toronto\EngSci\Year 4\Thesis\Designs\Latch Assembly V5\Latch PlusPlus.SLDPRT** Apr 8 21:56:33 2023

Study Properties

Study name	Static 1
Analysis type	Static
Mesh type	Solid Mesh
Thermal Effect:	On
Thermal option	Include temperature loads
Zero strain temperature	298 Kelvin
Include fluid pressure effects from SOLIDWORKS Flow Simulation	Off
Solver type	Automatic
Inplane Effect:	Off
Soft Spring:	Off
Inertial Relief:	Off
Incompatible bonding options	Automatic
Large displacement	On
Compute free body forces	On
Friction	Off
Use Adaptive Method:	Off
Result folder	SOLIDWORKS document (C:\Users\Ryan\OneDrive - University of Toronto\EngSci\Year 4\Thesis\Designs\Latch Assembly V5)

Units

Unit system:	SI (MKS)
Length/Displacement	mm
Temperature	Kelvin
Angular velocity	Rad/sec
Pressure/Stress	N/m^2

Material Properties

Model Reference	Properties	Components
	Name: Tough V5 **Model type:** Linear Elastic Isotropic **Default failure criterion:** Max von Mises Stress **Yield strength:** 6.06e+07 N/m^2 **Tensile strength:** 5.57e+07 N/m^2 **Elastic modulus:** 1.6e+09 N/m^2 **Poisson's ratio:** 0.35 **Mass density:** 1,200 kg/m^3 **Shear modulus:** 2.7e+09 N/m^2	SolidBody 1(Fillet10)(Latch PlusPlus)
Curve Data:N/A		

Loads and Fixtures

Fixture name	Fixture Image	Fixture Details
Fixed-1		**Entities:** 3 face(s) **Type:** Fixed Geometry

Resultant Forces

Components	X	Y	Z	Resultant
Reaction force(N)	-1.45299	14.9728	-0.00661151	15.0431
Reaction Moment(N.m)	0	0	0	0

Fixture name	Fixture Image	Fixture Details
Fixed-2		**Entities:** 1 face(s) **Type:** Fixed Geometry

Resultant Forces

Components	X	Y	Z	Resultant
Reaction force(N)	-3.88012	9.6919	0.00605844	10.4397
Reaction Moment(N.m)	0	0	0	0

Load name	Load Image	Load Details
Force-1		**Entities:** 1 face(s) **Type:** Apply normal force **Value:** 30 N

Connector Definitions

No Data

Interaction Information

No Data

Mesh information

Mesh type	Solid Mesh
Mesher Used:	Blended curvature-based mesh
Jacobian points for High quality mesh	16 Points
Maximum element size	1.04639 mm
Minimum element size	0.100728 mm
Mesh Quality	High

Mesh information - Details

Total Nodes	4086
Total Elements	2279
Maximum Aspect Ratio	4.4327
% of elements with Aspect Ratio < 3	99.1
Percentage of elements with Aspect Ratio > 10	0
Percentage of distorted elements	0
Time to complete mesh(hh;mm;ss):	00:00:02
Computer name:	

Sensor Details
No Data

Resultant Forces

Reaction forces

Selection set	Units	Sum X	Sum Y	Sum Z	Resultant
Entire Model	N	-5.33311	24.6647	-0.000553086	25.2347

Reaction Moments

Selection set	Units	Sum X	Sum Y	Sum Z	Resultant
Entire Model	N.m	0	0	0	0

Free body forces

Selection set	Units	Sum X	Sum Y	Sum Z	Resultant
Entire Model	N	0	0	0	0

Free body moments

Selection set	Units	Sum X	Sum Y	Sum Z	Resultant
Entire Model	N.m	0	0	0	0

Beams
No Data

Study Results

Name	Type	Min	Max
Stress1	VON: von Mises Stress	3.428e+04N/m^2 Node: 3837	3.719e+07N/m^2 Node: 2542

Latch PlusPlus-Static 1-Stress-Stress1
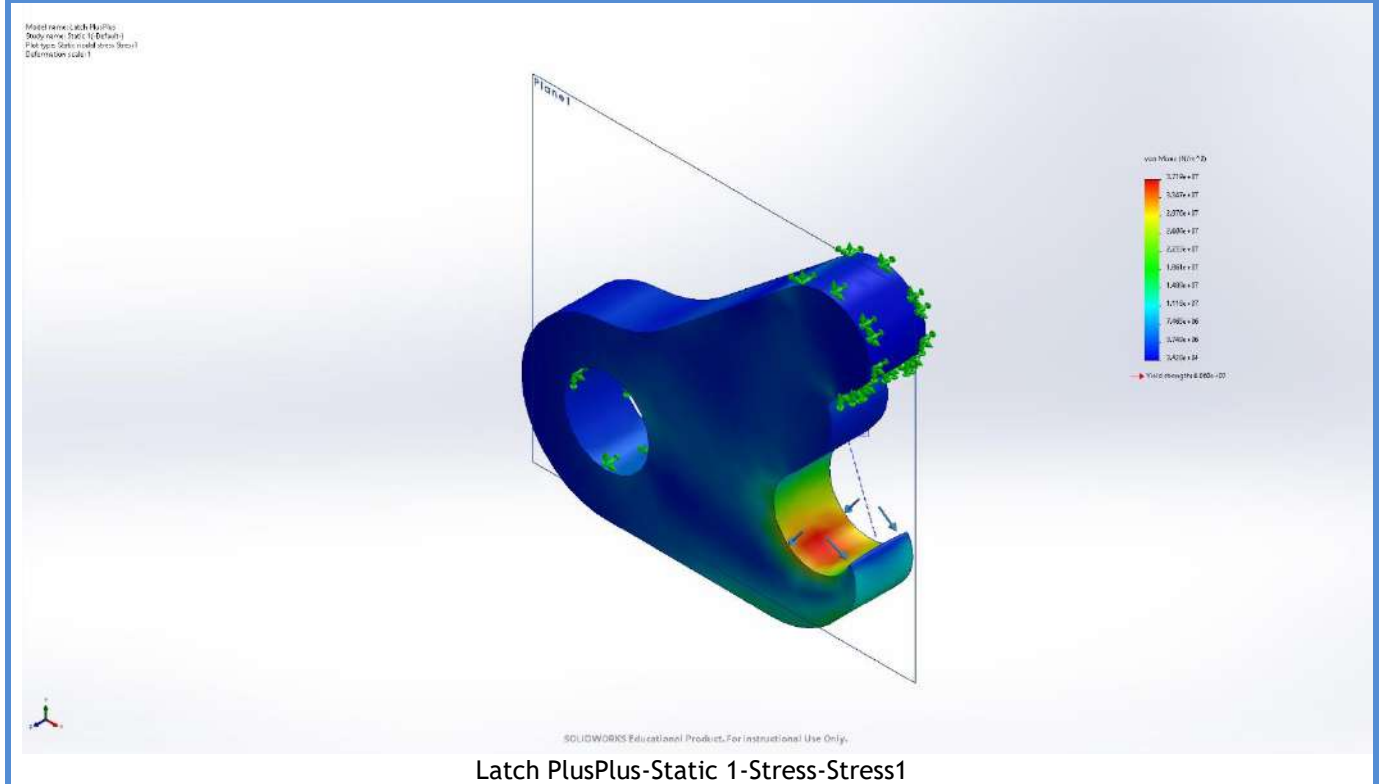
Name	Type	Min	Max
Displacement1	URES: Resultant Displacement	0.000e+00mm Node: 5	1.832e-01mm Node: 2736

Latch PlusPlus-Static 1-Displacement-Displacement1
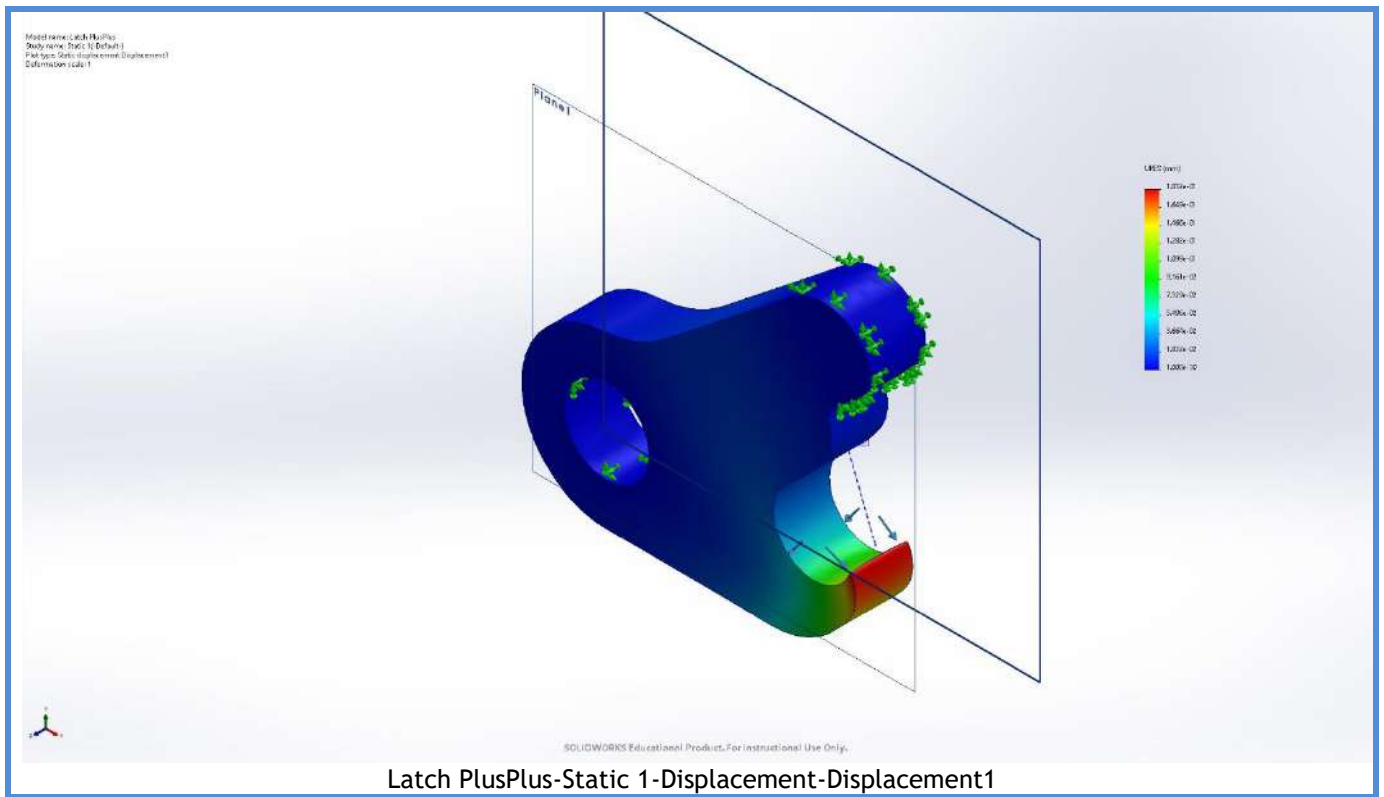
Name	Type	Min	Max
Strain1	ESTRN: Equivalent Strain	4.175e-05 Element: 2141	1.827e-02 Element: 1571

Latch PlusPlus-Static 1-Strain-Strain1

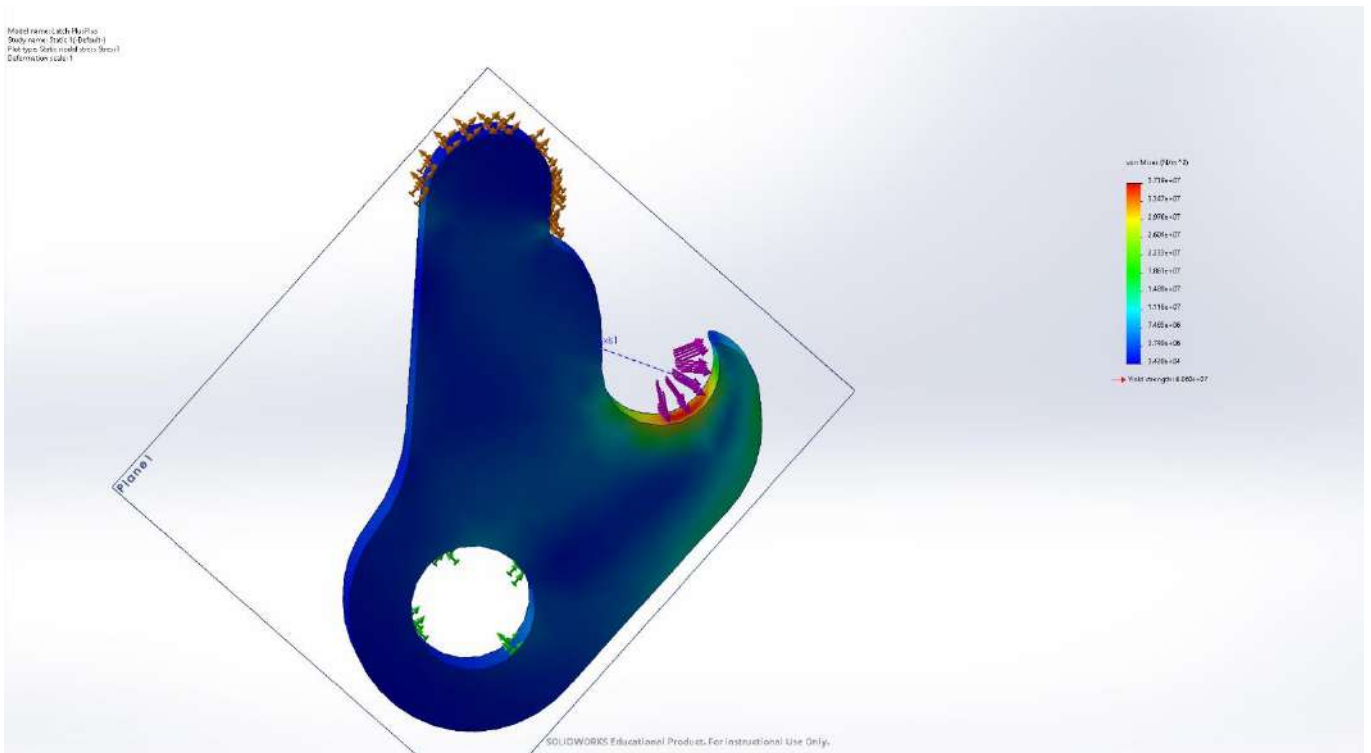| Name	Type
Displacement1{1}	Deformed shape
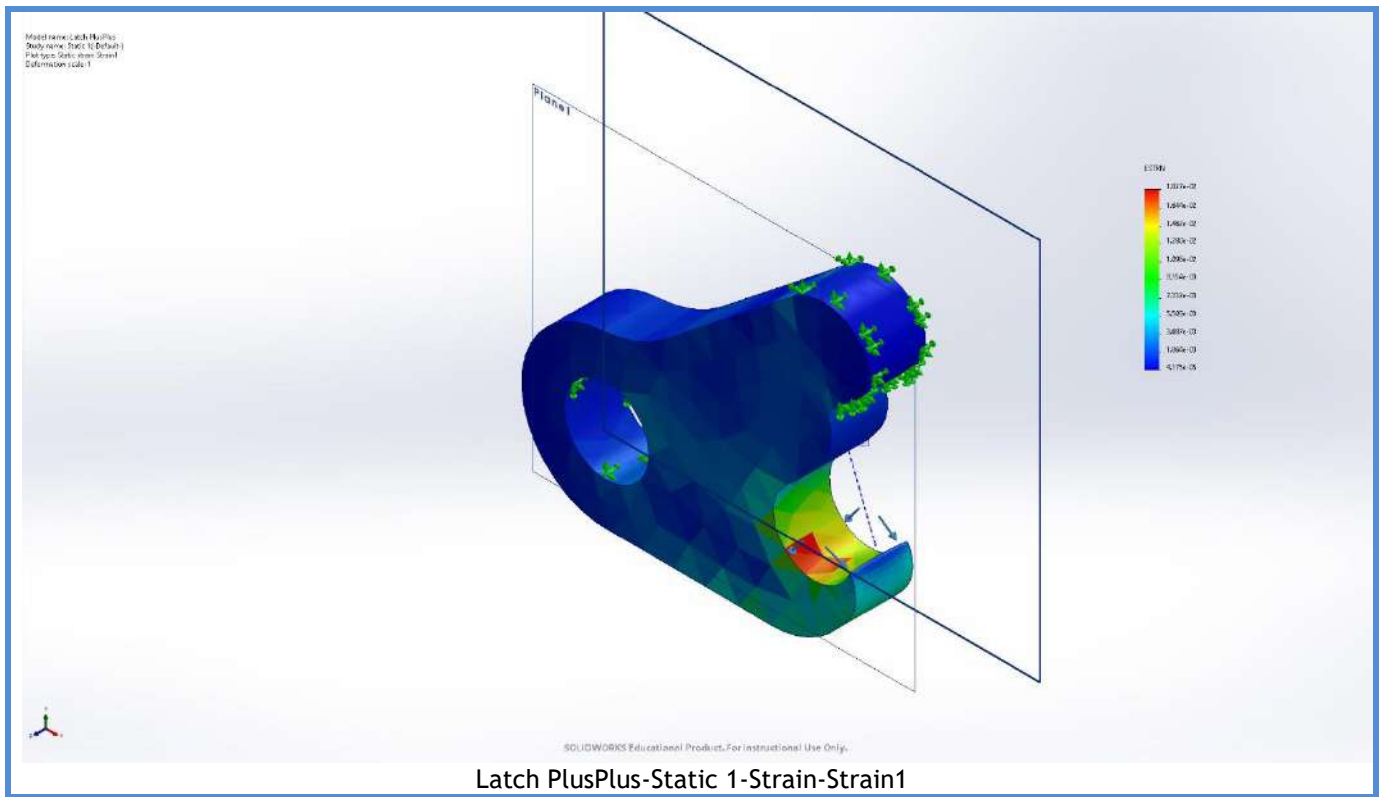
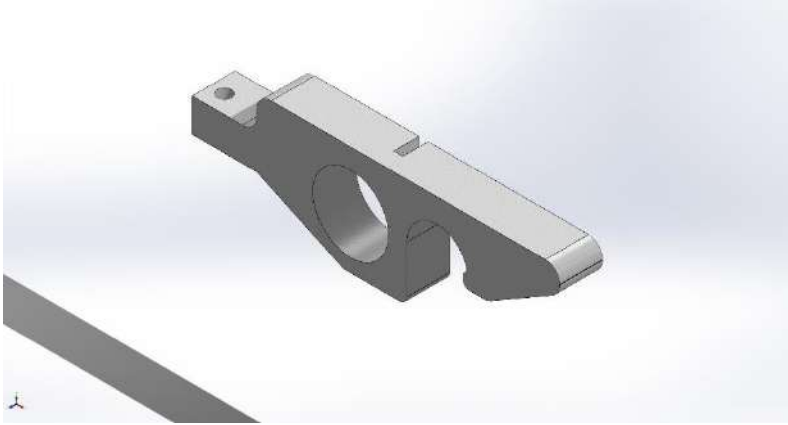Latch PlusPlus-Static 1-Displacement-Displacement1{1}
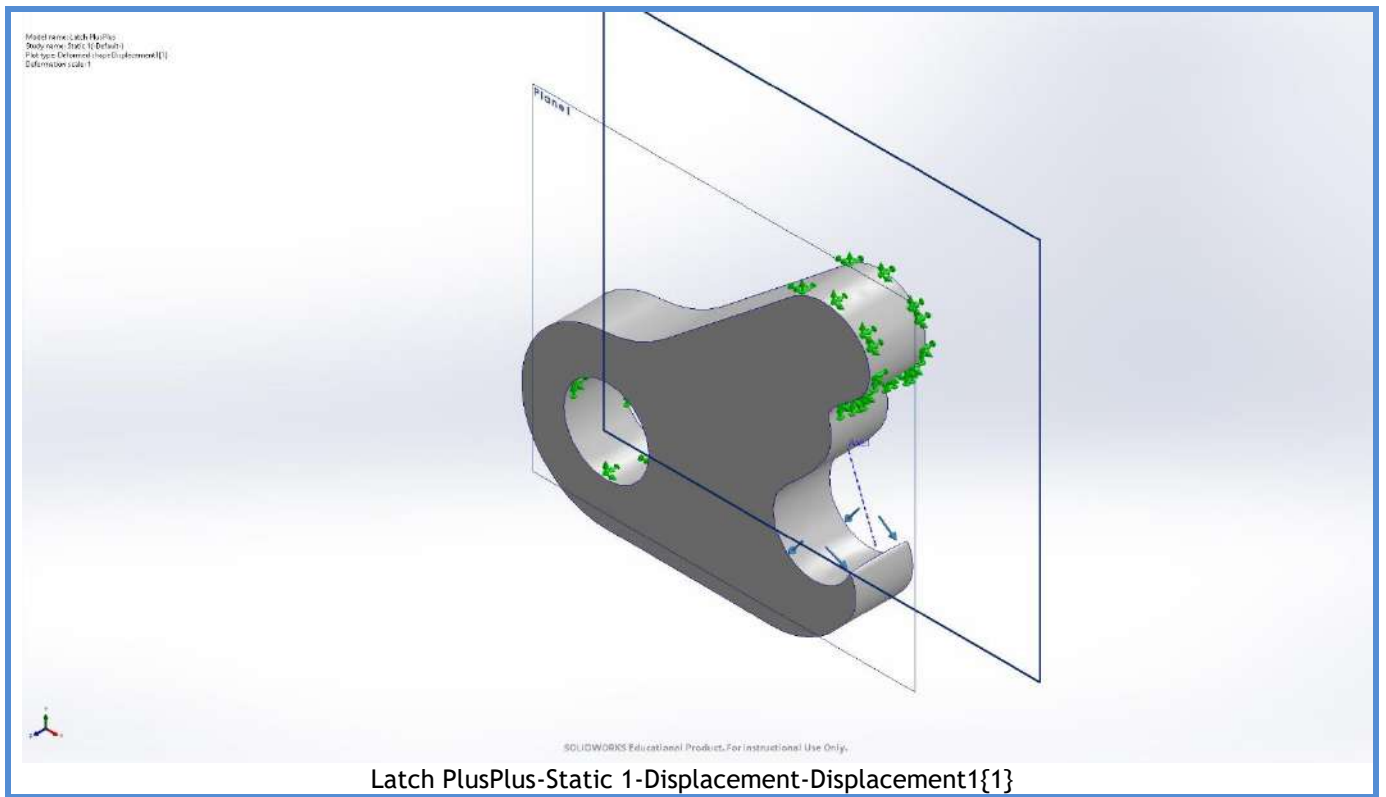
Image-1

Conclusion

Appendix

C Appendix C: Lock FEA Simulation Report

Simulation of Lock Plus Plus

Date: April 11, 2023
Designer: Ryan Zazo
Study name: Static 1
Analysis type: Static

Table of Contents

Description

No Data

Assumptions

Model Information

Model name: Lock Plus Plus
Current Configuration: Default

Solid Bodies

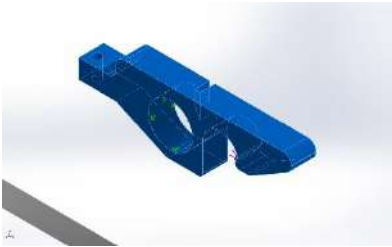| Document Name and Reference	Treated As	Volumetric Properties	Document Path/Date Modified
Fillet3	Solid Body	**Mass:0.000315525 kg Volume:2.62938e-07 m^3 Density:1,200 kg/m^3 Weight:0.00309215 N**	**C:\Users\Ryan\OneDrive - University of Toronto\EngSci\Year 4\Thesis\Designs\Latch Assembly V5\Lock Plus Plus.SLDPRT** Jan 30 01:02:15 2023

Study Properties

Study name	Static 1
Analysis type	Static
Mesh type	Solid Mesh
Thermal Effect:	On
Thermal option	Include temperature loads
Zero strain temperature	298 Kelvin
Include fluid pressure effects from SOLIDWORKS Flow Simulation	Off
Solver type	Automatic
Inplane Effect:	Off
Soft Spring:	Off
Inertial Relief:	Off
Incompatible bonding options	Automatic
Large displacement	On
Compute free body forces	On
Friction	Off
Use Adaptive Method:	Off
Result folder	SOLIDWORKS document (C:\Users\Ryan\OneDrive - University of Toronto\EngSci\Year 4\Thesis\Designs\Latch Assembly V5)

Units

Unit system:	SI (MKS)
Length/Displacement	mm
Temperature	Kelvin
Angular velocity	Rad/sec
Pressure/Stress	N/m^2

Material Properties

Model Reference	Properties	Components
	Name: Tough V5 **Model type:** Linear Elastic Isotropic **Default failure criterion:** Max von Mises Stress **Yield strength:** 6.06e+07 N/m^2 **Tensile strength:** 5.57e+07 N/m^2 **Elastic modulus:** 1.6e+09 N/m^2 **Poisson's ratio:** 0.35 **Mass density:** 1,200 kg/m^3 **Shear modulus:** 2.7e+09 N/m^2	SolidBody 1(Fillet3)(Lock Plus Plus)
Curve Data:N/A		

Loads and Fixtures

Fixture name	Fixture Image	Fixture Details
Fixed-1		**Entities:** 1 face(s) **Type:** Fixed Geometry

Resultant Forces

Components	X	Y	Z	Resultant
Reaction force(N)	-27.5672	11.1968	-1.60933e-06	29.7543
Reaction Moment(N.m)	0	0	0	0

Load name	Load Image	Load Details
Force-1		**Entities:** 1 face(s) **Type:** Apply normal force **Value:** 30 N

Connector Definitions
No Data

Interaction Information

No Data

Mesh information

Mesh type	Solid Mesh
Mesher Used:	Blended curvature-based mesh
Jacobian points for High quality mesh	16 Points
Maximum element size	0.640969 mm
Minimum element size	0.213654 mm
Mesh Quality	High

Mesh information - Details

Total Nodes	16973
Total Elements	10570
Maximum Aspect Ratio	14.74
% of elements with Aspect Ratio < 3	99.5
Percentage of elements with Aspect Ratio > 10	0.151
Percentage of distorted elements	0
Time to complete mesh(hh;mm;ss):	00:00:03
Computer name:	

Sensor Details

No Data

Resultant Forces

Reaction forces

Selection set	Units	Sum X	Sum Y	Sum Z	Resultant
Entire Model	N	-27.5672	11.1968	-1.60933e-06	29.7543

Reaction Moments

Selection set	Units	Sum X	Sum Y	Sum Z	Resultant
Entire Model	N.m	0	0	0	0

Free body forces

Selection set	Units	Sum X	Sum Y	Sum Z	Resultant
Entire Model	N	0	0	0	0

Free body moments

Selection set	Units	Sum X	Sum Y	Sum Z	Resultant
Entire Model	N.m	0	0	0	0

Beams
No Data

Study Results

Name	Type	Min	Max
Stress1	VON: von Mises Stress	1.709e+00N/m^2 Node: 10232	5.345e+07N/m^2 Node: 13141

Lock Plus Plus-Static 1-Stress-Stress1
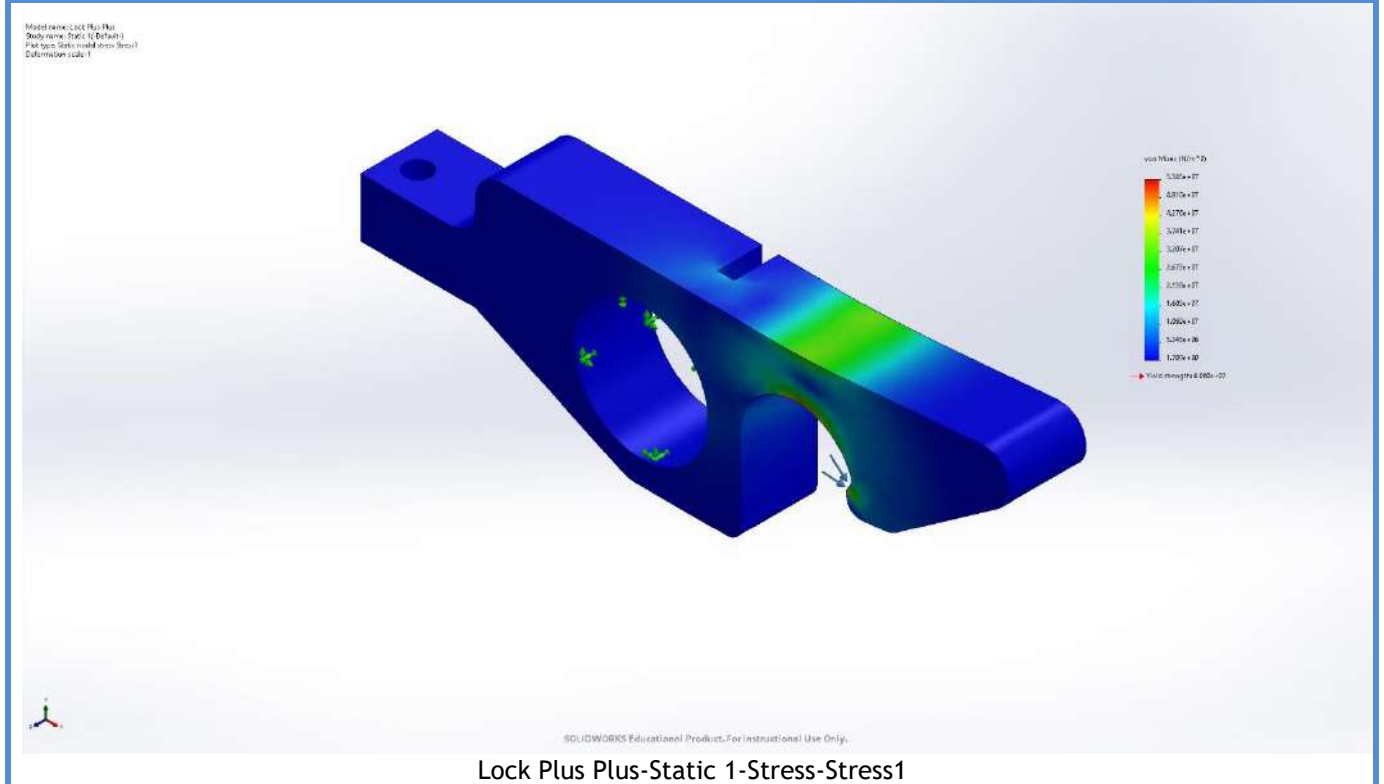
Name	Type	Min	Max
Displacement1	URES: Resultant Displacement	0.000e+00mm Node: 1	7.032e-01mm Node: 39

Lock Plus Plus-Static 1-Displacement-Displacement1
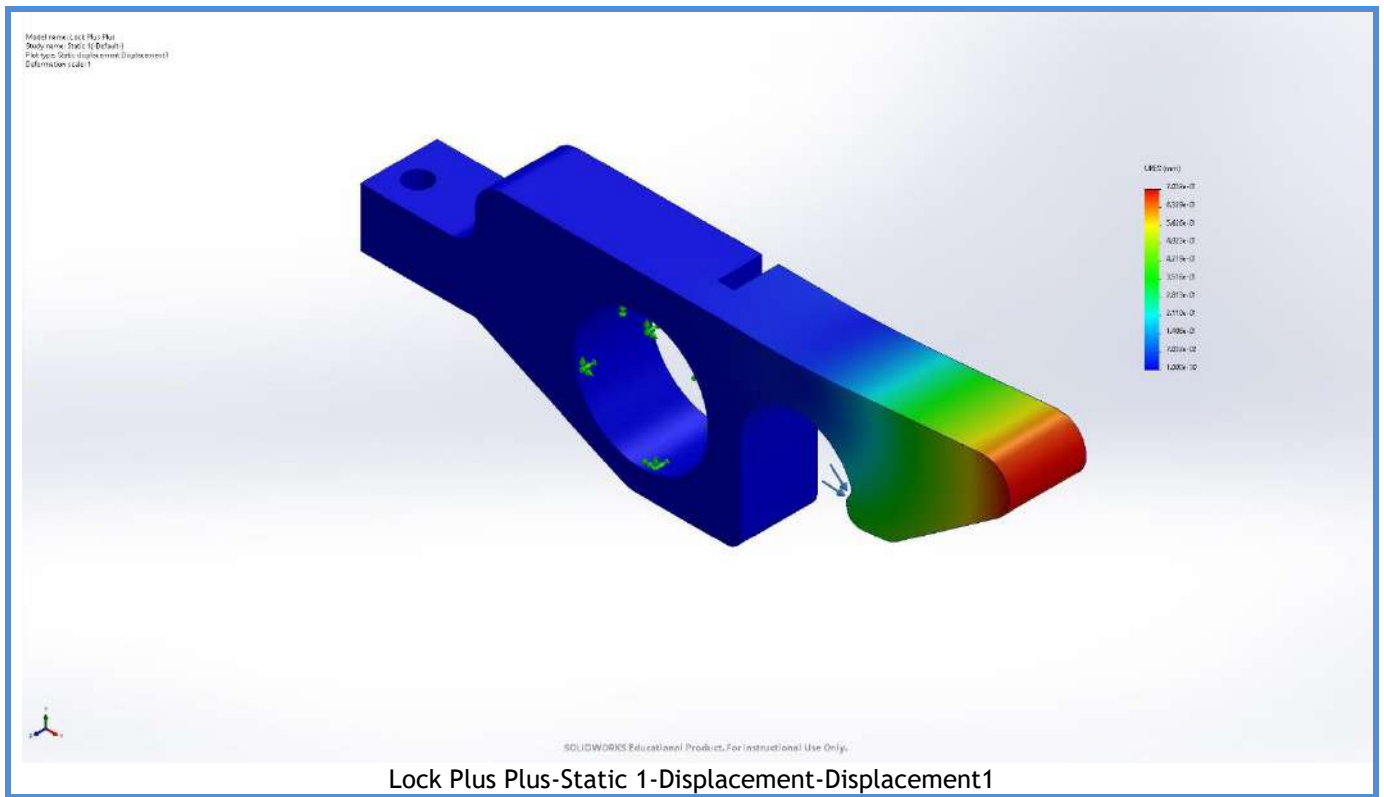
Name	Type	Min	Max
Strain1	ESTRN: Equivalent Strain	9.321e-10 Element: 5231	2.477e-02 Element: 9537

Model name: Lock Plus Plus
Study name: Static 1 (Default)
Plot type: Static strain Strain1
Deformation scale: 1

Lock Plus Plus-Static 1-Strain-Strain1

Name	Type
Displacement1{1}	Deformed shape

Model name: Lock Plus Plus
Study name: Static 1(Default)
Plot type: Deformed shape Displacement1[1]
Deformation scale: 1

SOLIDWORKS Educational Product. For Instructional Use Only.

Lock Plus Plus-Static 1-Displacement-Displacement1{1}
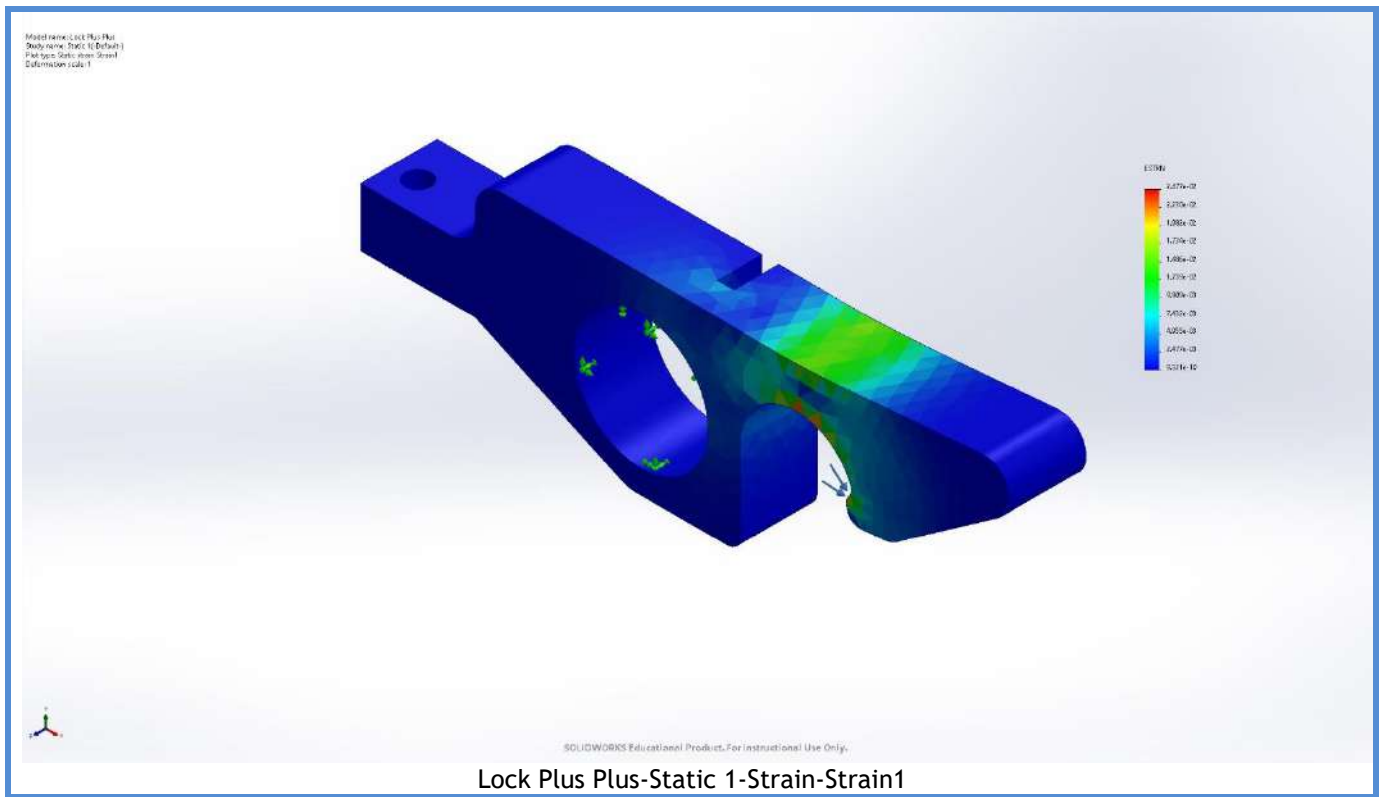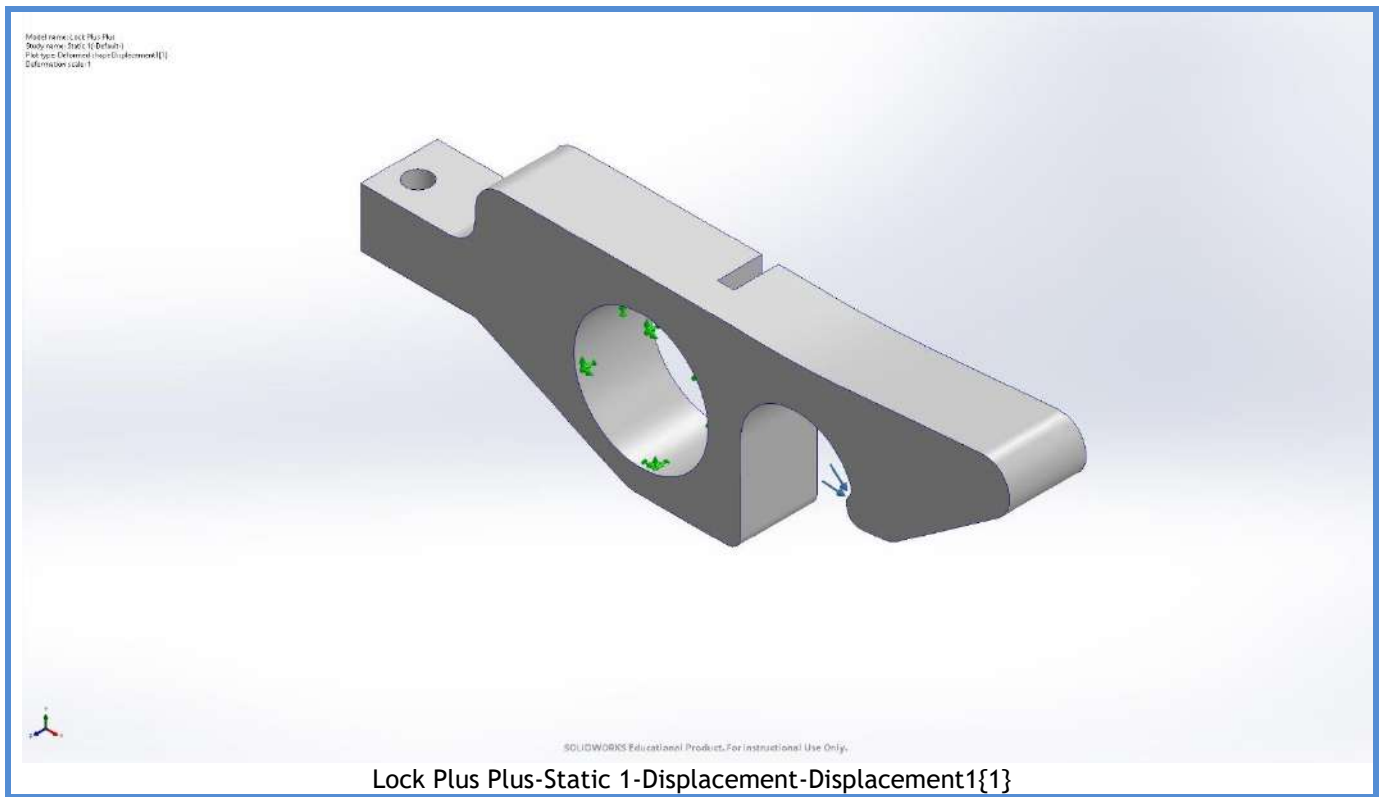
Conclusion

D Appendix D: System FEA Simulation Report

Simulation of LatchAssembly V5

Date: April 11, 2023
Designer: Ryan Zazo
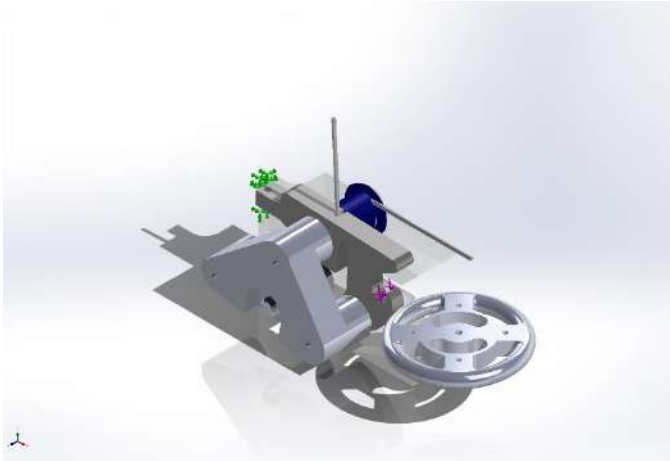**Study name:** Static 3
Analysis type: Static

Table of Contents

Description

No Data

Assumptions

Original Model
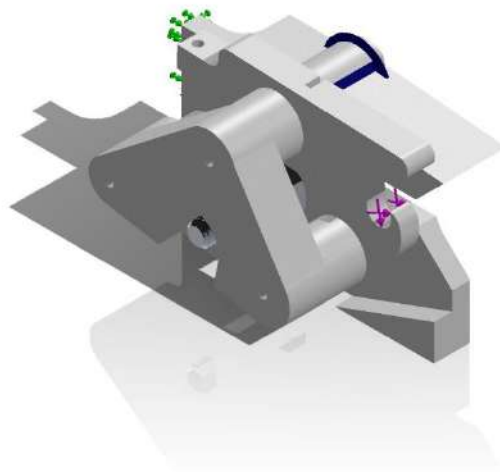

Model Analyzed

Model Information

Model name: LatchAssembly V5
Current Configuration: Default

Solid Bodies

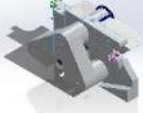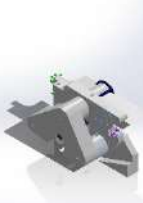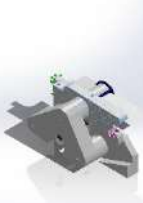| Document Name and Reference	Treated As	Volumetric Properties	Document Path/Date Modified
Extrude8	Solid Body	Mass:0.000290179 kg Volume:1.07474e-07 m^3 Density:2,699.98 kg/m^3 Weight:0.00284375 N	C:\Users\Ryan\OneDrive - University of Toronto\EngSci\Year 4\Thesis\Designs\Latch Assembly V5\98952A103_Aluminum Male-Female Threaded Hex Standoff.SLDPRT Jan 29 21:40:33 2023
Cut-Extrude17	Solid Body	Mass:0.0011736 kg Volume:9.77999e-07 m^3 Density:1,200 kg/m^3 Weight:0.0115013 N	C:\Users\Ryan\OneDrive - University of Toronto\EngSci\Year 4\Thesis\Designs\Latch Assembly V5\ClosingPlate.SLDPRT Jan 30 01:02:18 2023
Fillet2	Solid Body	Mass:0.00189771 kg Volume:1.58142e-06 m^3 Density:1,200 kg/m^3	C:\Users\Ryan\OneDrive - University of Toronto\EngSci\Year

		Weight:0.0185975 N	4\Thesis\Designs\Latch Assembly V5\Connecting Plate v16.step.SLDPRT Feb 10 15:41:32 2023
Fillet11	Solid Body	Mass:0.00016741 kg Volume:1.39508e-07 m^3 Density:1,200 kg/m^3 Weight:0.00164062 N	C:\Users\Ryan\OneDrive - University of Toronto\EngSci\Year 4\Thesis\Designs\Latch Assembly V5\Latch PlusPlus.SLDPRT Apr 11 18:55:41 2023
Fillet3	Solid Body	Mass:0.000315525 kg Volume:2.62938e-07 m^3 Density:1,200 kg/m^3 Weight:0.00309215 N	C:\Users\Ryan\OneDrive - University of Toronto\EngSci\Year 4\Thesis\Designs\Latch Assembly V5\Lock Plus Plus.SLDPRT Jan 30 01:02:15 2023

Study Properties

Study name	Static 3
Analysis type	Static
Mesh type	Solid Mesh
Thermal Effect:	On
Thermal option	Include temperature loads
Zero strain temperature	298 Kelvin
Include fluid pressure effects from SOLIDWORKS Flow Simulation	Off
Solver type	Automatic
Inplane Effect:	Off
Soft Spring:	Off
Inertial Relief:	Off
Incompatible bonding options	Automatic
Large displacement	Off
Compute free body forces	On
Friction	Off
Use Adaptive Method:	Off
Result folder	SOLIDWORKS document (C:\Users\Ryan\OneDrive - University of Toronto\EngSci\Year 4\Thesis\Designs\Latch Assembly V5)

Units

Unit system:	SI (MKS)
Length/Displacement	mm
Temperature	Kelvin
Angular velocity	Rad/sec
Pressure/Stress	N/m^2
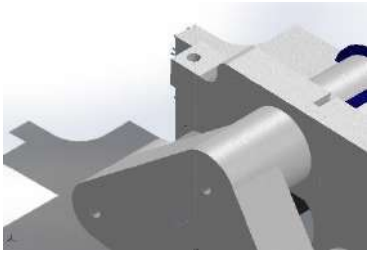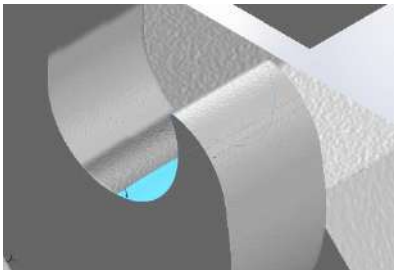
Material Properties

Model Reference	Properties	Components
	Name: 1060 Alloy **Model type:** Linear Elastic Isotropic **Default failure criterion:** Unknown **Yield strength:** 2.75742e+07 N/m^2 **Tensile strength:** 6.89356e+07 N/m^2 **Elastic modulus:** 6.9e+10 N/m^2 **Poisson's ratio:** 0.33 **Mass density:** 2,700 kg/m^3 **Shear modulus:** 2.7e+10 N/m^2 **Thermal expansion coefficient:** 2.4e-05 /Kelvin	SolidBody 1(Extrude8)(98952A103_Aluminum Male-Female Threaded Hex Standoff-1)
Curve Data:N/A		
	Name: Tough V5 **Model type:** Linear Elastic Isotropic **Default failure criterion:** Max von Mises Stress **Yield strength:** 6.06e+07 N/m^2 **Tensile strength:** 5.57e+07 N/m^2 **Elastic modulus:** 1.6e+09 N/m^2 **Poisson's ratio:** 0.35 **Mass density:** 1,200 kg/m^3 **Shear modulus:** 2.7e+09 N/m^2	SolidBody 1(Cut-Extrude17)(ClosingPlate-1), SolidBody 1(Fillet2)(Connecting Plate v16.step-1), SolidBody 1(Fillet11)(Latch PlusPlus-1), SolidBody 1(Fillet3)(Lock Plus Plus-1)
Curve Data:N/A		

Loads and Fixtures
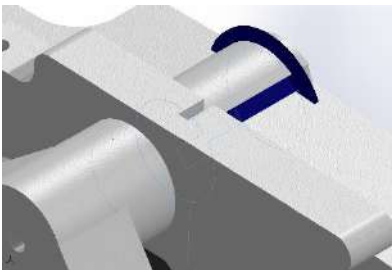
Fixture name	Fixture Image	Fixture Details
Fixed-1		**Entities:** 1 face(s) **Type:** Fixed Geometry

Resultant Forces

Components	X	Y	Z	Resultant
Reaction force(N)	-22.0342	12.3316	1.26362e-05	25.2502
Reaction Moment(N.m)	0	0	0	0

Load name	Load Image	Load Details
Force-1		**Entities:** 1 face(s) **Type:** Apply normal force **Value:** 30 N

Connector Definitions

Pin/Bolt/Bearing Connector

Model Reference	Connector Details	Strength Details
Pin Connector-1	**Entities:** 2 face(s) **Type:** Pin **With retaining ring (No translation):** Yes **With key (No rotation):** No **Connection Type:** Distributed **Units:** SI **Rotational stiffness value:** 0.03	No Data

Connector Forces Joint 1
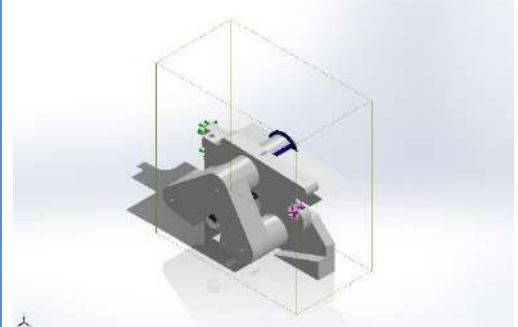
Type	X-Component	Y-Component	Z-Component	Resultant
Axial Force (N)	-0	-0	4.7594	-4.7594
Shear Force (N)	17.331	0.61862	0	17.342
Torque (N.m)	0	0	-0.00079412	0.00079412
Bending moment (N.m)	-0.011096	-0.0034967	0	0.011634

Connector Forces Joint 2

Type	X-Component	Y-Component	Z-Component	Resultant
Axial Force (N)	0	0	-4.7594	4.7594
Shear Force (N)	-17.331	-0.61862	0	17.342
Torque (N.m)	-0	-0	0.00079412	-0.00079412
Bending moment (N.m)	0.014028	-0.078652	0	0.079893

Interaction Information

Interaction	Interaction Image	Interaction Properties
Global Interaction		**Type:** Contact (Surface to surface) **Components:** 1 component(s)

Mesh information

Mesh type	Solid Mesh
Mesher Used:	Blended curvature-based mesh
Jacobian points for High quality mesh	16 Points
Maximum element size	2.87345 mm
Minimum element size	0.143672 mm
Mesh Quality	High
Remesh failed parts independently	Off

Mesh information - Details

Total Nodes	26216
Total Elements	14834
Maximum Aspect Ratio	152.54
% of elements with Aspect Ratio < 3	88.4
Percentage of elements with Aspect Ratio > 10	4.53
Percentage of distorted elements	0
Time to complete mesh(hh;mm;ss):	00:00:08
Computer name:	

Sensor Details
No Data

Resultant Forces

Reaction forces

Selection set	Units	Sum X	Sum Y	Sum Z	Resultant
Entire Model	N	-22.0342	12.3316	1.26362e-05	25.2502

Reaction Moments

Selection set	Units	Sum X	Sum Y	Sum Z	Resultant
Entire Model	N.m	0	0	0	0

Free body forces

Selection set	Units	Sum X	Sum Y	Sum Z	Resultant
Entire Model	N	-3.94881e-07	1.37463e-06	4.65289e-06	4.86774e-06

Free body moments

Selection set	Units	Sum X	Sum Y	Sum Z	Resultant
Entire Model	N.m	0	0	0	1e-33

Beams
No Data

Study Results

Name	Type	Min	Max
Stress1	VON: von Mises Stress	5.048e-02N/m^2 Node: 3361	4.234e+07N/m^2 Node: 25276

Model name: LatchAssembly V5
Study name: Static 3(-Default-)
Plot type: Static nodal stress Stress1
Deformation scale: 1

von Mises (N/m^2)

LatchAssembly V5-Static 3-Stress-Stress1
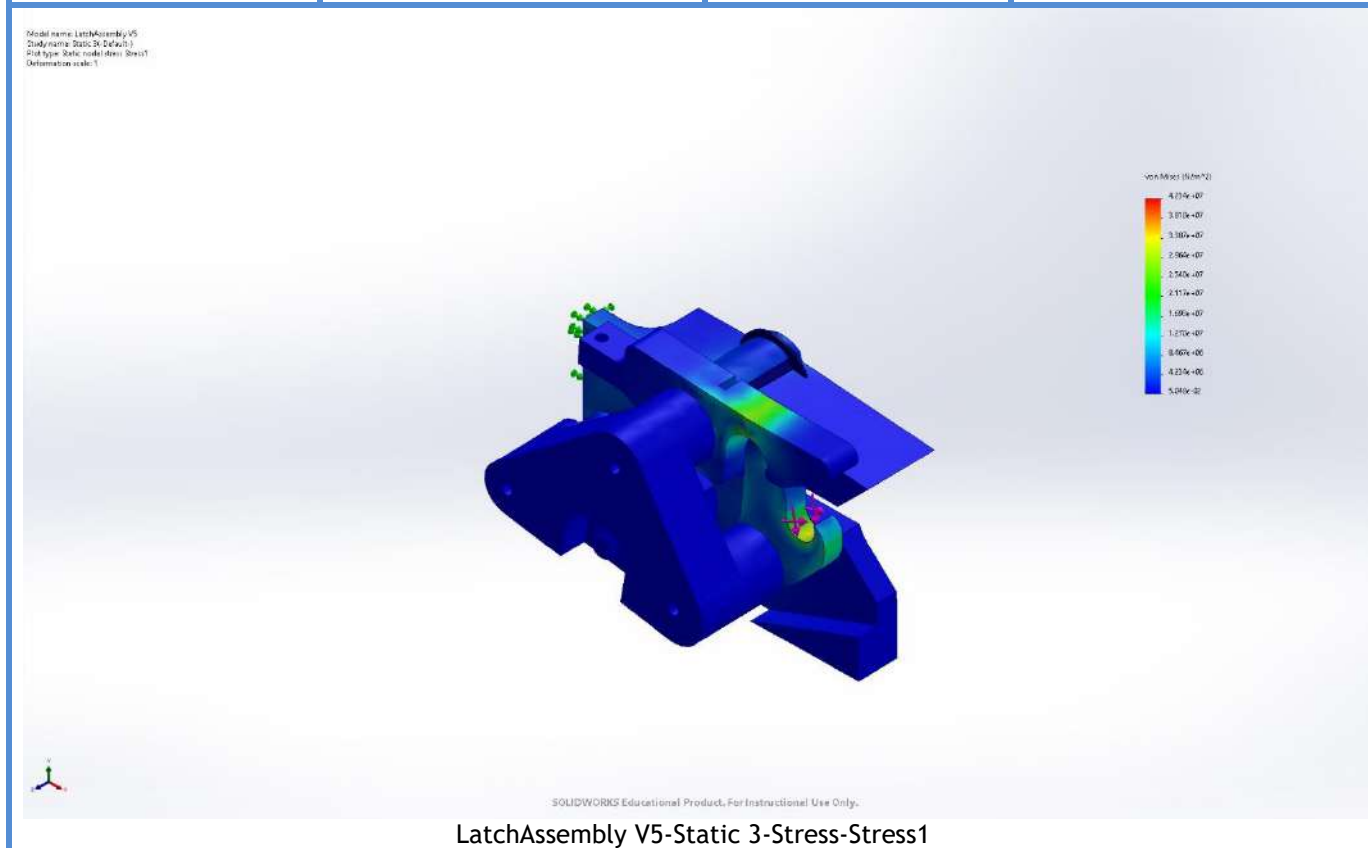
Name	Type	Min	Max
Displacement1	URES: Resultant Displacement	0.000e+00mm Node: 13079	7.104e-01mm Node: 18031

Model name: LatchAssembly V5
Study name: Static 3t-Default-)
Plot type: Static displacement Displacement1
Deformation scale: 1

URES (mm)

LatchAssembly V5-Static 3-Displacement-Displacement1
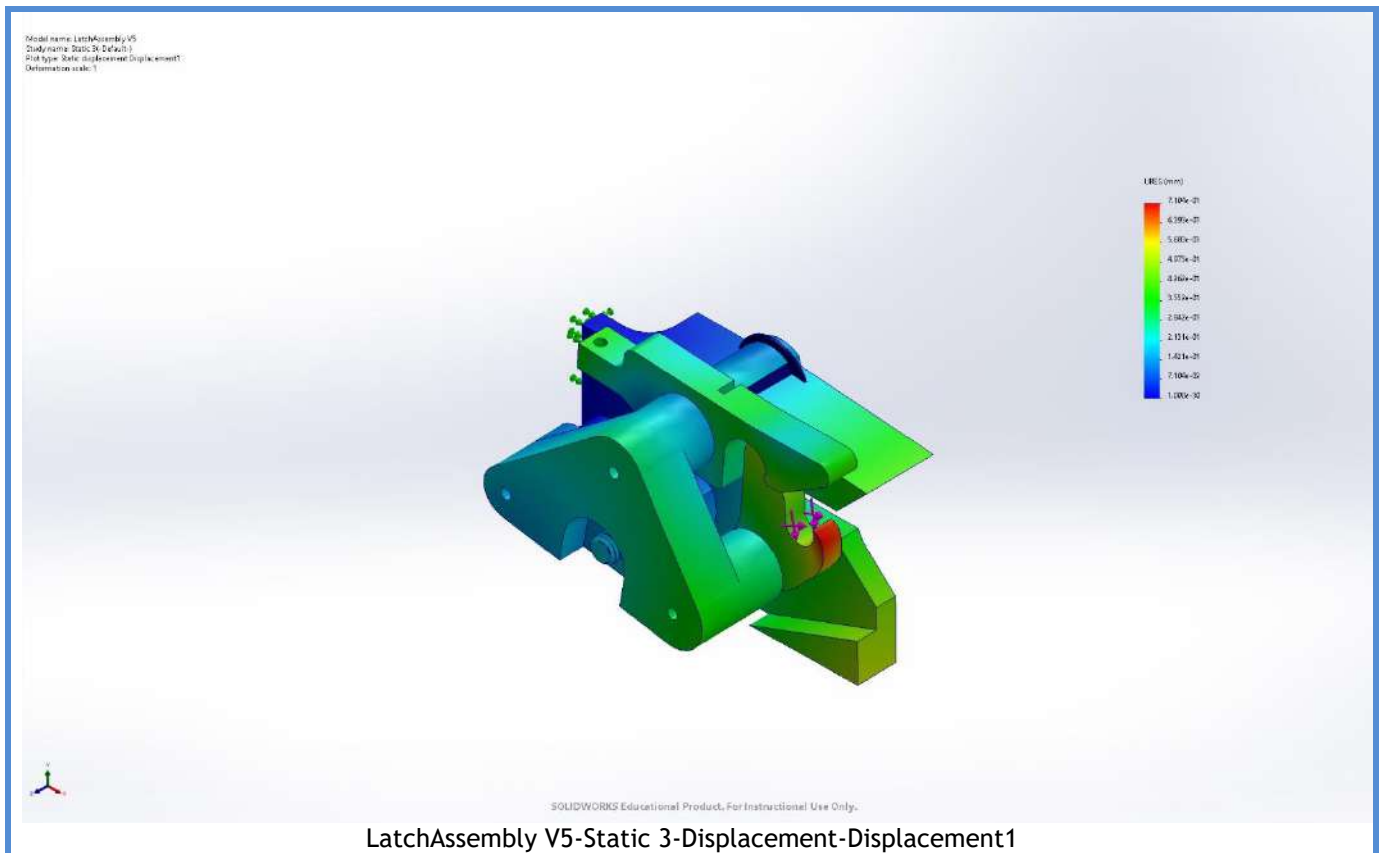
Name	Type	Min	Max
Strain1	ESTRN: Equivalent Strain	6.123e-13 Element: 1100	1.797e-02 Element: 13807

Model name: LatchAssembly V5
Study name: Static 3(-Default-)
Plot type: Static strain Strain1
Deformation scale: 1

ESTRN

1.795e-02
1.617e-02
1.437e-03
1.258e-02
1.078e-02
8.988e-03
7.190e-03
5.393e-03
3.595e-03
1.798e-03
6.125e-13

SOLIDWORKS Educational Product. For Instructional Use Only.

LatchAssembly V5-Static 3-Strain-Strain1

Name	Type
Displacement1{1}	Deformed shape

Model name: LatchAssembly V5
Study name: Static 3k-Default-)
Plot type: Deformed shape Displacement1{1}
Deformation scale: 1

SOLIDWORKS Educational Product. For Instructional Use Only.

LatchAssembly V5-Static 3-Displacement-Displacement1{1}

Conclusion

Appendix